

Review

Critical Review on Advanced Cooling Strategies in Friction Stir Processing for Microstructural Control

Md Saad Patel ^{1,2}, R. Jose Immanuel ^{2,3}, Ariful Rahaman ^{1,4,*}, Mohammad Faseeulla Khan ⁵  and Mustapha Jouiad ^{6,*} 

¹ School of Mechanical Engineering, Vellore Institute of Technology, Vellore 632014, Tamil Nadu, India; mdsaad.patel@vit.ac.in

² Advanced Material Development and Characterization Group, Indian Institute of Technology Bhilai, Kutelabhata, Durg 491001, Chhattisgarh, India; jose@iitbhilai.ac.in

³ Department of Mechanical Engineering, Indian Institute of Technology Bhilai, Kutelabhata, Durg 491001, Chhattisgarh, India

⁴ Centre for Materials Characterization and Testing, Vellore Institute of Technology, Vellore 632014, Tamil Nadu, India

⁵ Department of Mechanical Engineering, College of Engineering, King Faisal University, Al-Hasa 31982, Saudi Arabia; fmohammad@kfu.edu.sa

⁶ Laboratory of Physics of Condensed Matter (LPMC), University of Picardie Jules Verne, Scientific Pole, 33 Rue Saint-Leu, CEDEX 1, 80039 Amiens, France

* Correspondence: arahaman@vit.ac.in (A.R.); mustapha.jouiad@u-picardie.fr (M.J.)

Abstract: Friction stir processing (FSP) stands as an effective approach designed for grain refinement and site-specific microstructural modification. The evolving microstructure during FSP is determined by various variables out of which rate of sample cooling is the key parameter. More often, FSP is conducted in naturally flowing air; however, a large number of studies are conducted by researchers across the world; stressing the importance of additional sample cooling strategy for tailoring the material microstructure. Such strategies vary not only in terms of the cooling medium used but also with regard to various other compliant conditions that must be fulfilled for the cooling process to make them successful and economically viable. This work critically reviews the most prevalent methods practiced by various researchers and industries for controlled sample cooling during and after FSP. The underlying mechanisms; advantages; disadvantages; and limitations of each procedure along with the resulting microstructure and material performances are discussed and recommendations are provided

Keywords: friction stir processing; cooling strategy; grains refinement; microstructural modification; mechanical properties



Citation: Patel, M.S.; Immanuel, R.J.; Rahaman, A.; Khan, M.F.; Jouiad, M. Critical Review on Advanced Cooling Strategies in Friction Stir Processing for Microstructural Control. *Crystals* **2024**, *14*, 655. <https://doi.org/10.3390/cryst14070655>

Academic Editor: Umberto Prisco

Received: 26 June 2024

Revised: 9 July 2024

Accepted: 15 July 2024

Published: 17 July 2024



Copyright: © 2024 by the authors. Licensee MDPI, Basel, Switzerland. This article is an open access article distributed under the terms and conditions of the Creative Commons Attribution (CC BY) license (<https://creativecommons.org/licenses/by/4.0/>).

1. Introduction

The process of sculpting the microstructure and characteristics of the surface layer is an efficient way to improve the operational qualities of the components of machines and other machinery. The microstructure of the uppermost layer and product attributes are the result of surface change that occurred prior to product use, or they are the outcome of activities that take place while the product is being used [1–3]. The friction stir processing (FSP) technique is one of the most recently developed techniques in the field of surface engineering. This technique is basically derived from the friction stir welding (FSW) principle, it is used for grain refining, and it is mainly employed in metal processing [4]. The FSP technique involves inserting a rotating tool into the surface of a metal, which generates heat and plastic deformation, resulting in a refined grain structure that improves the mechanical performance of the material as depicted in Figure 1.

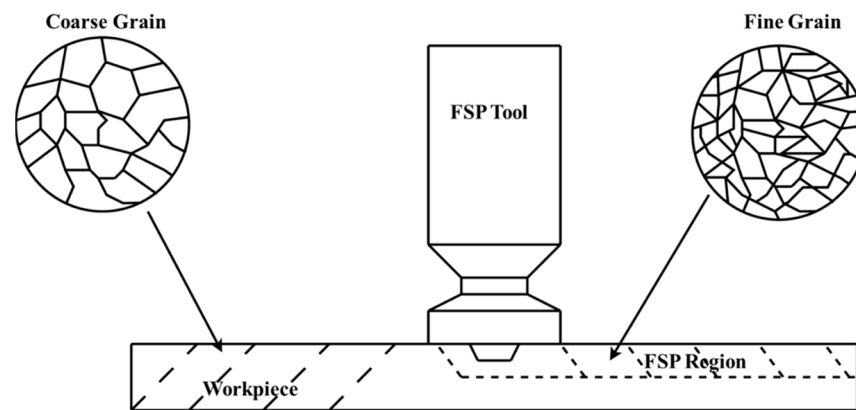


Figure 1. Schematic illustration of microstructural evolution during FSP.

The intense heat produced in the stirred zone (SZ) is typically in the range of 0.6–0.9 T_m , where T_m is the workpiece/specimen's melting temperature [5,6]. Established by [7,8], the FSP technique has potential applications in the aerospace, automotive, and marine industries, and nowadays, it is one of the most intriguing approaches for modifying the top layer of structural materials. It has been extensively investigated for several structural materials, including aluminum (Al) [9–14], magnesium (Mg) [15–20], titanium (Ti) [21–25], copper (Cu) [26–30], and steel [31–36]. Figure 2 shows statistics on the number of publications, both research articles and review papers, in the previous two decades.

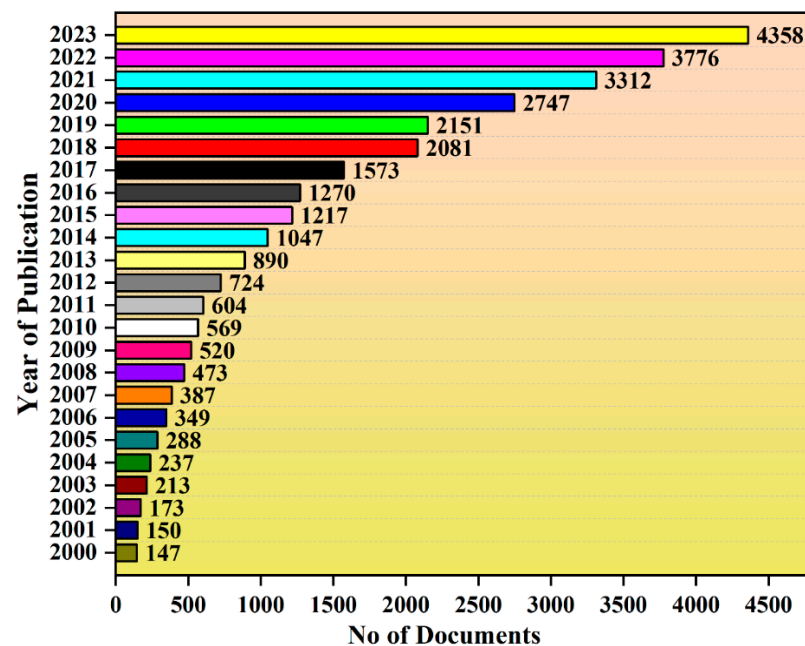


Figure 2. Number of publications per year involving FSP technique.

In FSP technology, all the metallurgical changes in the material occur exclusively in the solid state, and friction between the tool and the workpiece generates the majority of the heat. However, volumetric heating caused by plastic deformation also considerably adds to the total heat generated during the operation [37]. A major part of the friction heat produced in FSP is through the shoulder/work material interaction and a small percentage of contribution comes from the tool pin/work material. This makes tool design an important and inevitable stage in planning the process strategy in the FSP [38,39]. The level of heat produced is subsequently determined by the process parameters, specifically the traverse and tool rotating speeds [40].

The enhancement of the processing parameters such as tool speed and feed rate, could improve to some extent the material's cooling rate during the processing; however, further improvement is limited by the material's intrinsic properties and the efficiency of the cooling medium used. Supplying additional cooling medium possessing a higher degree of cooling concentration is generally used for FSP treatment to improve the mechanical [41,42], wear [43,44], corrosion [45,46], and superplastic [47] properties. While working with materials that have low melting points, such as Al or Mg alloys [48,49], it is a common practice to use additional cooling techniques to prevent material properties alteration. The method recently developed to improve the efficiency of the cooling rate and to further enhance the mechanical performance through restricting the processed material microstructure to fine grains (between 1 and 5 μm) or UFG ($<1 \mu\text{m}$), is to synchronously condition the sample while performing FSP [50,51]. Lately, a series of methodologies and cooling mediums have been used to boost the material's cooling rate. Table 1 provides a comparison of various cooling strategies in FSP.

Table 1. Comparison of cooling strategies in FSP.

Cooling Strategy	Advantages	Disadvantages
Natural air cooling	It is very simple, economical and requires no additional equipment.	Slower cooling rates, leading to variability in microstructure.
Water cooling	Quick cooling, easy to implement.	Thermal shock risk, possibility for corrosion
Air jet cooling	Quicker than natural air, reduced thermal shock.	Demands a compressed air system, slower than liquids.
Cryogenic cooling	Extremely quick cooling, refined and homogeneous grain structure.	Substantial costly, requires specialized equipment, and safety measures.
Heat sink method	Balanced cooling, fits specified geometries.	Limited to simple geometries.
Active cooling	Highly customizable, enhanced efficiency.	High complexity and cost, precise control needed.

From Table 1, the four most prevalent methods (air cooling, water cooling, cryogenic cooling, and heat sink) have been shortlisted for further detailed review. Compressed air was the first to be investigated [52,53], followed by carbon dioxide (CO_2) gas, which gained an incredible recognition since it displayed a phase transition of liquid CO_2 to dry ice, followed by heat absorption to convert dry ice back into CO_2 . This process allows for the absorption of a significant amount of heat during the FSP. To date, the liquid CO_2 approach has been shown to enable cooling rates of 500–1000 k/s [54,55]. As CO_2 is a primary greenhouse gas, it has a high potential to form surface oxides when reacting with certain materials at high temperatures, hence its use as a cooling medium is limited. Water was used as a cooling media by many researchers [56,57], followed by liquid nitrogen (LN) since it displays a higher cooling capacity when compared with other cooling media [58,59]. As far as the cooling medium must have a greater heat capability to absorb heat effectively and sufficient specific conductance to prevent overheating, it is equally essential to possess limited reactivity. Indeed, the cooling agent should not interact with the work material and lead to undesired alteration to the working material. The use of a cooling medium during FSP helps to lower the temperatures of both the workpiece and the tool. This reduction in temperature mitigates thermal damage to both components, thereby prolonging the lifespan of the tool and improving the overall quality of the treated material [60]. The highest degree to which the tool is heated during FSP with air cooling, as well as the repeated heating cycles, significantly contribute to the tool's rapid wear [61]. The technique of cooling a material is greatly determined by the choice of cooling agent. The most investigated options include submerging the rotating tool and the specimen in coolant or

spraying coolant on the tool/workpiece interaction [62–70]. The use of heat sinks such as Cu or steel blocks below the work material is rarely reported [71,72]. Figure 3 illustrates the cooling media and techniques utilized in recent FSP studies.

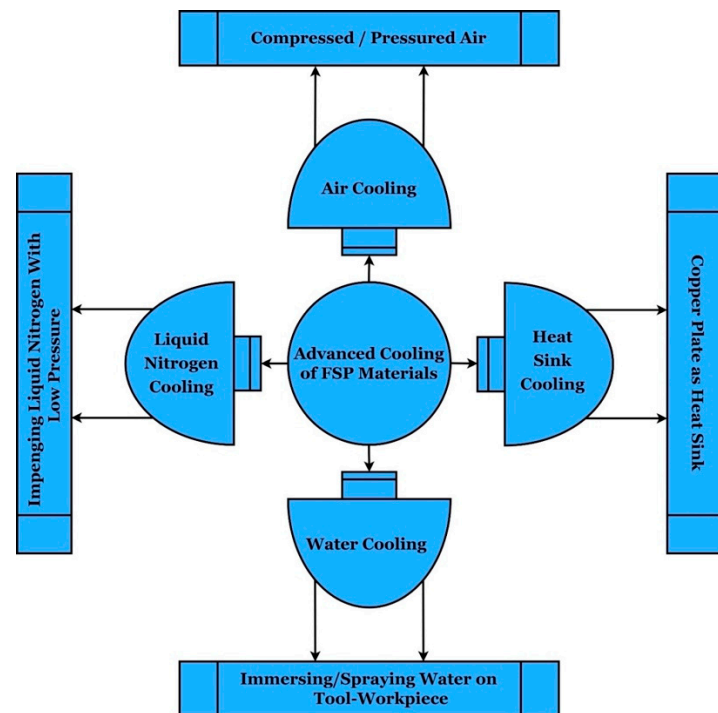


Figure 3. Widely utilized cooling techniques in FSP.

In the case of lightweight and low melting alloys, the addition of a cooling process frequently results in significant grain refinement and better material structural homogeneity. These microstructural alterations are linked to the improvements of certain mechanical properties such as tensile strength and hardness. However, it is critical to consider that the impact of cooling procedures might vary depending on the material system and the specific property under consideration. This in turn contributes to the improvement of the overall mechanical properties of the material. Keeping in mind how quickly FSP technology is evolving and the existing numerous ways to cool the material are rapidly growing, this study provides insights into the methods including different cooling media explored by various researchers to quickly cool the material during and after FSP. This review article describes not only cooling solutions and treatments but also the various types of cooling agents, including their benefits and drawbacks and instances in which they could be used. This report intends to assist in selecting the most effective FSP method and cooling solutions for specific materials based on their application.

2. Advanced Cooling Techniques and Agents

2.1. Air Cooling

Air is frequently employed as a cooling agent in FSP technologies. It has been investigated by many researchers. Due to its favorable specific heat capacity, it can provide effective cooling with a quick reduction in the temperature of the treated area [73]. One of the most compelling reasons to use air as a cooling media is that it is inexpensive and does not have any technical criteria that must be met for it to be stored or transported to the processing area, as is the case with certain other cooling agents, such as dry ice and LN, etc. Furthermore, the use of air as a cooling agent is environmentally friendly and cost-effective compared to other cooling methods, making it a popular choice in various industries. The most common method of using air for cooling is to impinge it with moderate to high velocity on the tool/workpiece area while performing FSP as depicted in Figure 4. Hybrid

FSP was demonstrated to be used as an active cooling technique to generate equiaxed fine-grain at the SZ by reducing the processing temperature through utilizing pressurized air assistance during single pass FSP of AA7075 Al alloy (5.75 Zn–2.66 Mg–1.79 Cu–0.24 Cr balance Al in wt.%) [74]. The compressed air-cooled sample was found to have shown good grain refinement of 3.0 μm in comparison to the naturally cooled sample. This was mainly due to an improved cooling rate of 0.48 $^{\circ}\text{C}/\text{s}$ observed in the case of compressed air samples. This led to an excellent performance of superplastic elongation of 367% in comparison to 233% of naturally cooled samples.

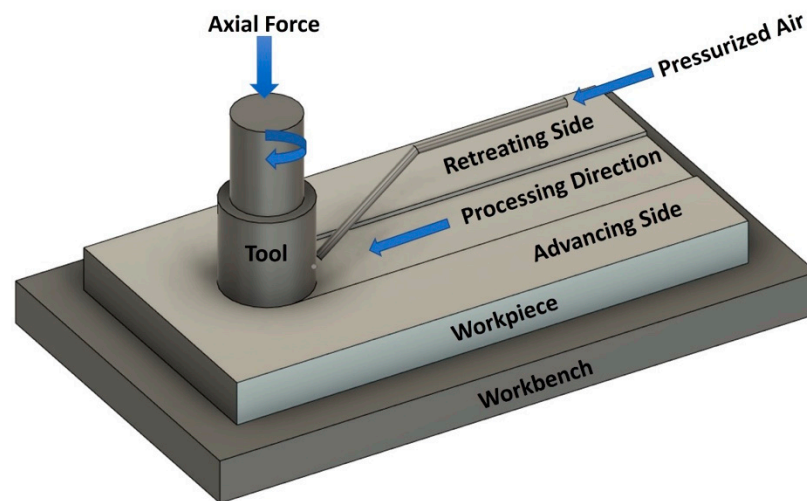


Figure 4. Schematics of FSP under pressurized air cooling.

Similar findings were observed in [75], where they processed as-cast A356 (7 Si–0.31 Fe–0.2 Cu–0.1 Mn–0.3 Mg–0.1 Zn–0.25 Ti balance Al in wt.%) and examined how varying cooling conditions, including coolants and flow rates impact the temperature, wear resistance, applied forces, mechanical characteristics, and microstructural features during FSP of the Al–Si Al alloy. Specifically, the study focused on the FSP that was executed with several flow rates of compressed air and water coolants, each of which had its own unique characteristics. The amount of force generated during FSP was experimentally quantified with the use of a load-measuring instrument that was specifically constructed for this purpose. An increase in FSP axial force was observed due to a decrease in temperature brought on by an increase in the cooling rate. The magnitude of this increase was proportional to the degree to which the temperature dropped. The sample subjected to FSP that was generated using cooling media had a smaller average size for the Si particles than the specimen that underwent FSP that had not been fabricated using the cooling technique. An increase in the cooling rate caused both the decrease in average Si particle size and an upsurge in aspect ratio at the agitated zone. The mean Vickers hardness (HV) of the samples, subjected to FSP produced by air cooling were significantly higher than those produced by natural cooling. When compared to the A356 base alloy, the wear mass loss in the specimens after FSP was much reduced. It was discovered that the predominant wear mechanism for each of the samples was either the abrasive wear or delamination wear component.

An investigation was conducted on the microstructure and selected characteristics of the Al 7075 alloy that has been exposed to FSP with the use of chill cooling air at various angles (i.e., 45 $^{\circ}$ and 90 $^{\circ}$) between the workpiece and the air nozzle [76]. The study reported a unique approach to cooling the sample during FSP. It involved using an air stream chilled to –11 $^{\circ}\text{C}$ through a jet cooling nozzle as shown in Figure 5a. The novel cooling technique is more effective than cooling in still air, evident from the changes in the microstructure that are more favorable, improved mechanical characteristics, and wear resistance. It is observed that the utilization of a jet cooling nozzle, which speeds up the cooling process, resulted in increased grain refinement from 240 μm to 3.2 μm when the jet impinged at 90 $^{\circ}$,

and 1.4 μm when the jet impinged at 45° , as depicted in Figure 5b–d. This refinement is significantly higher compared to the refinement obtained under still air conditions, which is 7.6 μm . Such a refined microstructure resulted in an increase in HV of about 19.2% and 17.1% for 45° and 90° jet impingement angles, respectively.

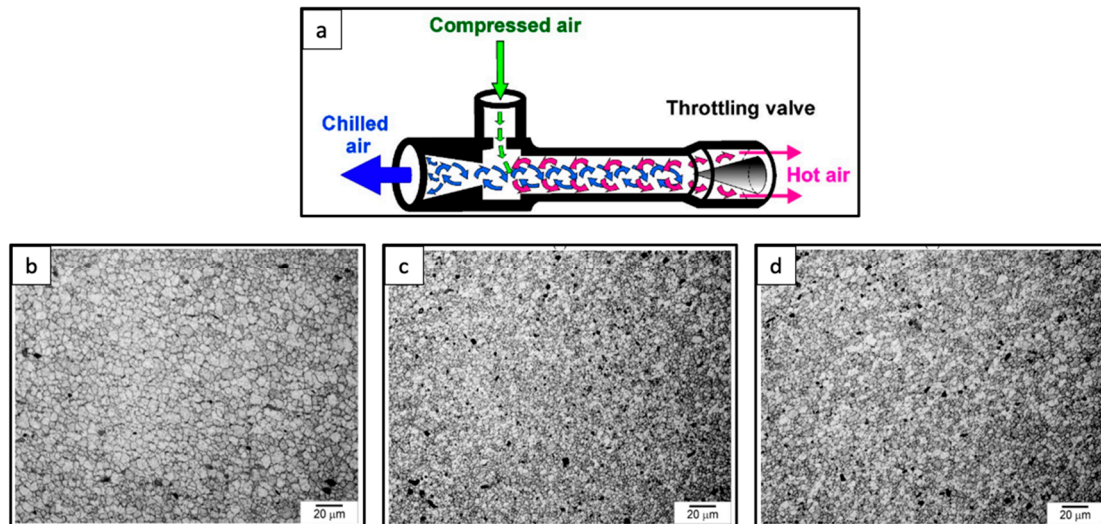


Figure 5. (a) Jet cooling nozzle, microstructures (b) without cooling, (c) 45° sample, (d) 90° sample [76].

Another group worked on the effect of air cooling on the FSP of Mg alloy [77]. They subjected the AZ91 Mg alloy (8.5 Al–0.7 Zn–0.32 Mn–0.01 Si–0.001 Cu–0.001 Fe balance Mg in wt%) to FSP with the help of jet cooling air. The material subjected to FSP with air chilling displayed excellent grain refinement with an average grain size of 1.4 μm whereas a 9 μm grain size was obtained for samples without the cooling system as shown in Figure 6a,b. The use of a jet cooling nozzle made it possible to achieve a higher level of grain refinement, particularly in terms of the surface area. In the SZ, coarsening of the microstructure was avoided by maintaining a greater cooling rate. Enhancement of HV and advancements in the ability to resist wear of AZ91 alloy after FSP with air cooling was observed, which was due to the favorable changes in the microstructure.

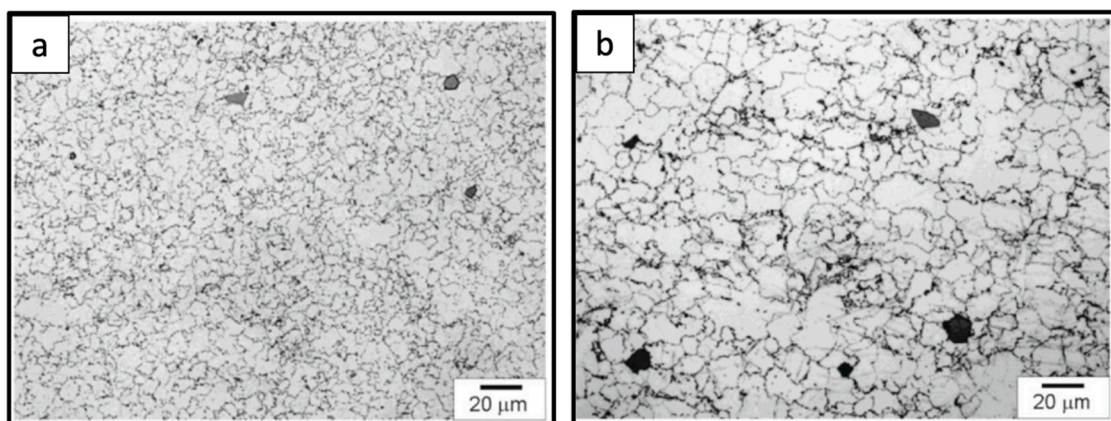


Figure 6. Microstructures of AZ91 after FSP: (a) air-cooled and (b) naturally cooled [77].

NiAl Bronze alloy [78] was subjected to FSP with an air blower as a media of cooling, and significant grain refinement was observed, which in turn resulted in a surge in HV value from 150 to 280 VHN. The elimination of the heat-building effect that is associated with the friction process during FSP in conjunction with simultaneous cooling of the processed zone

in the material was achieved by a jet cooling nozzle this holds particular importance when considering the application of multi-band treatment. Since this treatment is carried out in dry circumstances, it eliminates the challenge of dealing with the removal of liquid coolant from the processing location. The proposed cooling solution can be implemented in real-world scenarios without the need for extensive and expensive modifications or adjustments to the workstation. The results reported in the literature so far have demonstrated that the jet cooling nozzle is quite effective in its mission to cool the treated zone. Therefore, this approach could serve as a viable substitute for current methods employed in FSP technology, offering the prospect of innovative pathways in the fabrication of FSP-treated materials.

2.2. Water Cooling

The physical properties of water are significantly superior to those of air when it comes to the usage of both as a cooling medium. Water has a higher specific heat capacity than air. As a result, water transfers heat more efficiently. A 1 L amount of water can extract three thousand times more energy from a system than 1 L of air [79]. The cooling capacity and availability of water will not be affected in any way by dirt or dust since it is a closed process system. With all the above-mentioned advantages, one drawback of using water is its ability to corrode materials such as steel [80] and Mg [81]. Hence, caution must be taken when selecting water as a cooling medium during FSP, particularly when dealing with materials that are highly susceptible to corrosion in a water-based setting. It is important to note that the destructive effect of water in the context of FSP treatment is rarely observed, even when water-immersed processing is used. During FSP, no indication of corrosion was encountered in the friction-modified zone of AZ80 Mg alloy entirely submerged in water at room temperature [82]. The most common method of using water for cooling is to submerge both the tool and the workpiece in water, or alternatively, apply a water spray onto the surface as shown in Figure 7.

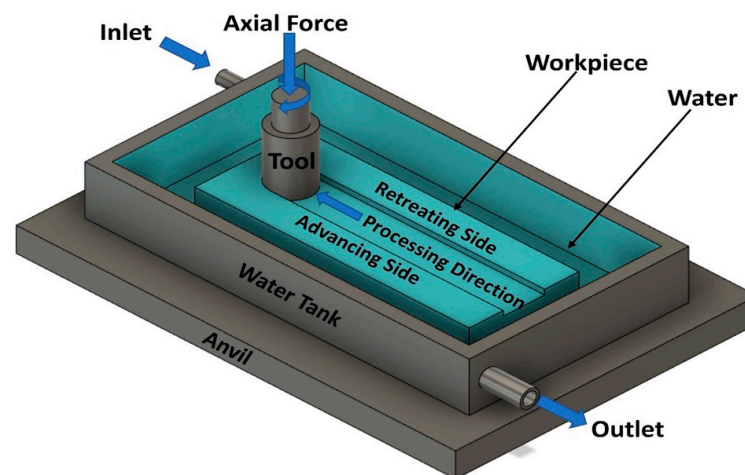


Figure 7. Schematic illustration of submerged FSP.

The cooling effectiveness of the friction stir-treated specimen is noticeably higher when the water immersion method is utilized compared to the conventional still air cooling. This immersion processing technique was used [83] to investigate the fatigue properties of the AA6061 alloy that was processed by still air and submerged FSP at room temperature. Excellent grain size refinement was observed in the case of underwater FSP. Since FSP involves high temperatures, the operational material experiences a process of thermal annealing. Thermal annealing leads to mainly three softening phenomena: dynamic recovery, dynamic recrystallization, and grain growth. During the dynamic recovery process, the imperfection formed during the plastic deformation will tend to annihilate. Dislocations of opposing signs attract and destroy one other, while dislocations of like signs merge to transform into low-angle grain boundaries [84]. In the process of dynamic

recovery, the existing dislocations act as points for initiating dynamic recrystallization leading to the creation of a stir zone characterized by the formation of recrystallized grains devoid of strain and possessing a low dislocation density. Due to the elevated temperature, grain coarsening occurs in the recrystallized zone after recrystallization. The utilization of water serves to eliminate the heat generated at the interface of the sample tool, thereby controlling the coarsening of recrystallized grains during FSP. As a consequence, a highly fine-grained microstructure develops in submerged FSP as shown in Figure 8a–c, producing a greater proportion of high-angle grain boundaries than FSP without a cooling medium. The mechanical and fatigue performance of the AA6061 Al alloy, subjected to FSP was significantly enhanced when compared with base metal (BM) as reported by the authors, which was due to significant grain refinement.

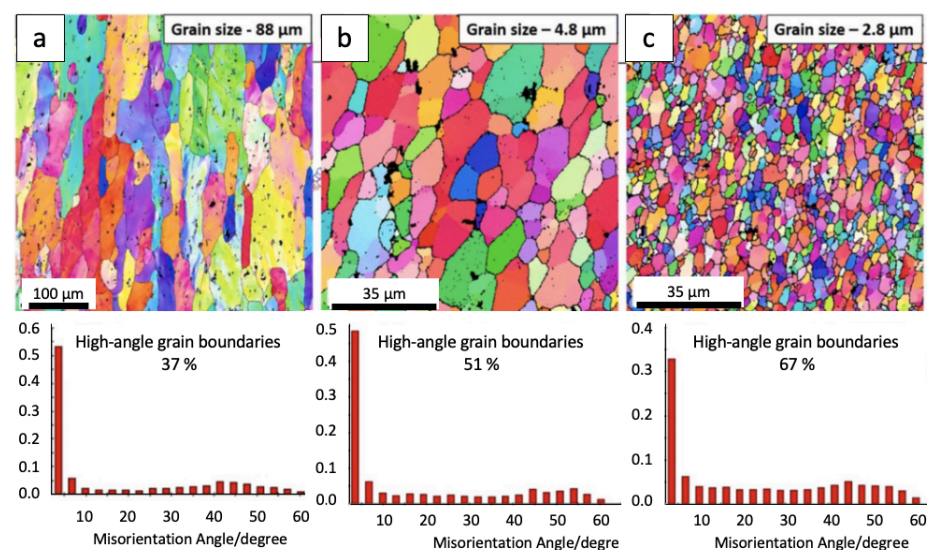


Figure 8. EBSD microstructures and grain misorientation maps of (a) BM, (b) FSP under ambient conditions, and (c) submerged FSP samples (reprinted with permission from [83]. Copyright © 2022 Elsevier).

FSP was performed on AA5083 in submerged environments [85], which revealed a dramatic grain refinement was accomplished with an average grain size of 3.9 μm from 67 μm due to the great cooling effect offered by water during FSP. The growth of fine grains was caused by uniform heat dispersion from the processing zone via the convection heat transfer mechanism. The SFSP specimen outperformed the BM in terms of corrosion resistance due to the formation of fine intermetallic and refined grain structures generated through FSP. Comparable results were reported [86] on superior tensile strength and wear resistance AZ31 Mg alloy through FSP. During FSP for swift cooling, water at a temperature of 10 $^{\circ}\text{C}$ was supplied to the processing area at a flow rate of 1.2 L/min, which resulted in a 57% increment in the HV and a 21% improvement in strength and minimum wear rate of the samples following FSP. The homogeneity of the Mg matrix and $\text{Mg}_{17}\text{Al}_{12}$ phase was the primary cause for the increase in HV after FSP. In addition, rapid cooling led to solid solution strengthening by the dissolution of the $\text{Mg}_{17}\text{Al}_{12}$ phase into the Mg, which further enhanced the HV. It was determined that microstructural refinement leading to increased HV, stronger work hardening ability, and enhanced ductility were the primary contributors to the decrease in wear rates for specimens following FSP. The effects of different pin profiles on the mechanical performance of AZ31B under immersion conditions were reported [87], where water was utilized as the cooling agent. The average grain size was found to be 1.99 μm for the scrolled stepped square pin profile and its grain structure following FSP became more homogenized and had a reduced grain size as a consequence of the decrease in the overall duration of the process as well as lowering the temperature during the process using an effective cooling system. Another group (Luo et al., [88])

studied the superplastic studies on multi-pass SFSP with an overlapping ratio of 50% of as-cast AZ61 and achieved equiaxed fine-grained structures with an average grain size of 4 μm . An excellent superplasticity of 467% was obtained at a strain rate of $1 \times 10^{-3}/\text{s}$ at 623 K, which primarily resulted from the swift reduction in temperature experienced by the sample during FSP which helped in suppressing the regrowth of irregular networks like $\beta\text{-Mg}_{17}\text{Al}_{12}$ phase which deteriorates the superplastic performance. Similarly, AZ91 [89] was subjected to SFSP to study the superplastic performance at a strain rate of $2 \times 10^{-2} \text{ s}^{-1}$ and 623 K, they achieved an exception elongation of 990% this was mainly attributed to refined microstructure and suppression of the secondary phase produced by controlled cooling during processing.

The FSP treatment is not exclusively applied to materials with a low melting point, like Al and Mg alloys, even though these are undoubtedly the most prevalent examples. By using a blend of water and ethanol in equal proportion as a submerged liquid media, ultra-fine grains (UFG) of SS316L were obtained [90]. The FSP fixture was coupled to an external chiller via the outlet and inlet ports for a roughly 100 mL/min constant supply of coolant as shown in Figure 9a. The material had a mean grain size of 22 μm before FSP. After single pass FSP, the mean grain size was reduced to 0.9 μm as depicted in Figure 9b,c, the refinement was mainly attributed to the recrystallization events that entailed the formation of a new grain structure via different nucleation and growth stages, which is known as discontinuous dynamic recrystallization. Because of the more refined grain size, a greater yield strength (YS) of 450 MPa was achieved.

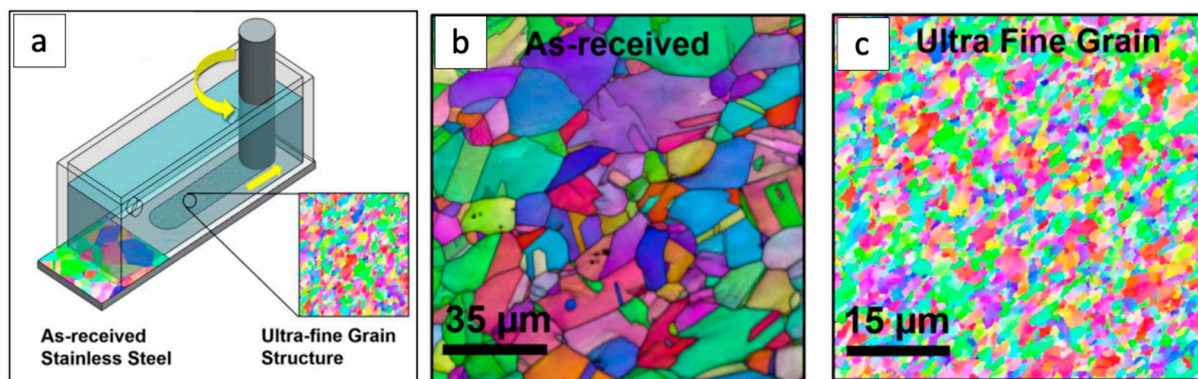


Figure 9. (a) Submerged FSP setup, EBSD microstructures of SS316L: (b) as-received (c) ultra-fine grain produced by submerged FSP [90].

Nickel, characterized by its elevated melting point underwent FSP [91]. To investigate the cooling of the workpiece, the researchers employed the water-immersed processing technique. Throughout the procedure, the sample was enveloped by a stream of water acting as a coolant to maintain consistent cooling. They aimed to assess the practicality of utilizing common tool steel for processing elevated melting temperature metals and to gauge the extent of tool wear during processing under conditions involving cooling in both still air and water. The performed study demonstrated that effectively treating nickel is achievable when subjected to rapid cooling conditions and most importantly, this procedure is not accompanied by considerable tool abrasion. In the instance of a comparable operation performed with cold air cooling, the tool was severely damaged owing to the fast increase in temperature during the process. Q235 low carbon steel subjected to SFSP was reported to yield a reduced average grain size from 11.3 μm to 7.8 μm [92]. A phase change occurred during the SFSP due to the rapid cooling of material by water. Initially, BM consists of ferrite and pearlite phases; however, in the case of SFSP, the temperature obtained was higher than the point at which ferrite begins to evolve into austenite. During the following cooling, some of the initial ferrite is converted into austenite and subsequently into martensite at this temperature range. Due to this refined microstructure and formation of the martensitic

phase, improvement in mechanical performance was achieved with an ultimate tensile strength (UTS) greater than 38.7% of BM.

The FSP technique is also an effective method for developing surface composites [93] into a laminar composite structure consisting of dynamic recrystallization of α phase layers and UFG β CuZn layers. The reinforcement induced in the material helps in improving the material's mechanical characteristics [94–98] as well as the resistance to wear [99] and corrosion [100,101], enabling a wider range of industrial applications.

Moreover, a variety of reinforcement materials such as, ZrC [102] SiC [103], Al₂O₃ [104], B₄C [105], BN [106] TiC [107], TiO₂ [108,109], TiB₂ [110], CNT [111], MWCNT [112], WC [113], Cr₂O₃, and Ni [114] were used to produce composites apart from the traditional production of hybrid composites. Other authors successfully fabricated AZ31 with Ca as an alloying material and hydroxyapatite as a reinforcement and found that it exhibited excellent corrosion properties [115]. A summary of the effect of water as a cooling media on mechanical properties reported by researchers is given in Table 2.

Table 2. Overview of improved grain size and mechanical performance reported following SFSP (A—artificial aging; NA—natural aging; O—annealing).

Alloy/Composite Designation	No of Passes	Average Grain Size		Mechanical Performance						Ref.
		Before FSP	After FSP	HV before FSP	HV after FSP	Tensile Strength before FSP	Tensile Strength after FSP	Elongation before FSP	Elongation after FSP	
		(μm)	(μm)	(HV)	(HV)	(MPa)	(MPa)	(%)	(%)	
AZ31	1	85.3	5.43	59	70	280	246	9.72	12.38	[116]
AZ31	4	10.2	3.2	63	86	275	349	24	20	[117]
AZ61	1	-	5.2	61	71	74	108	9.2	28.1	[118]
	2	5.2	4.6	71	70	108	100	28.1	37.2	
AZ61	2	-	10.6	55	64	151	238	12.52	31.7	[119]
AZ91	1	72	2.8	-	-	55	151	15.2	25.4	[120]
AZ91	1	72	1.2	63	101	105	310	15.2	30.9	[121]
LA103Z	1	90	20.25	56	89.1	177.9	305.5	36.1	4.1	[122]
Al 1060	1	19.71	0.690	36	66.3	70	95.2	-	-	[123]
	2	0.690	0.686	66	52	95.2	82	-	-	
	3	0.686	5.36	52	32	82	68	-	-	
Al-7B04 (AA)	1	-	1.77	177	150	560	528	10.3	13.9	[124]
Al-7B04 (O)	1	-	1.47	62	130	220	385	16.5	12.2	
Al5083	3	27	1.3	-	-	279	329	26.3	28.1	[125]
Al5083/Ti	3	27	1	-	-	279	432	26.3	23.2	
A356	1	-	2	72	88	124	231	14.15	1.30	[126]
A2014	1	-	2.48	84	170	246.7	475	-	12	[127]
Al 6061 (NA)	1	18	2.6	95	74	264	215	14.1	13.6	[128]
Al 6061 (O)	1	18	2.4	39	49	103	120	17.2	12.3	
Cu-Zn Plate	1	48.1	2.9	107	118	166	371	39	10.1	[129]
AA7075	2	-	3.0	-	104	-	-	-	-	[130]
AZ31/(ZrO ₂ + CuO)	-	-	4.09	75	124	-	161	-	1.2	[131]

2.3. Liquid Nitrogen Cooling

In FSP, LN is increasingly employed as a cooling medium. The increased heat capacity of LN compared to air and water enhances the pace of cooling during FSP. Typically, two strategies are applied to accomplish ultra-fast cooling using LN: (1) by immersing the sample into LN, and (2) by spraying it on the tool/workpiece surface throughout the process. Nevertheless, compared to other cooling mediums, LN is more complex to utilize and needs more care. Primarily, when LN encounters a material at a higher temperature it evaporates incredibly quickly, resulting in the creation of an insulating gas layer that lowers the cooling intensity [132]. The stability of the LN cooling process is partially compromised compared to traditional methods due to the presence of nitrogen gas generated by the cooling system. This makes it important to carefully monitor the cooling process and adjust the amount of LN being used to maintain the desired temperature [133]. Additionally, LN cooling systems can be more expensive to operate and require specialized equipment and proper handling. However, LN cooling is still preferred in industries due to its high cooling capacity and low environmental impact [134]. Figure 10 shows the working of FSP under LN in spray mode.

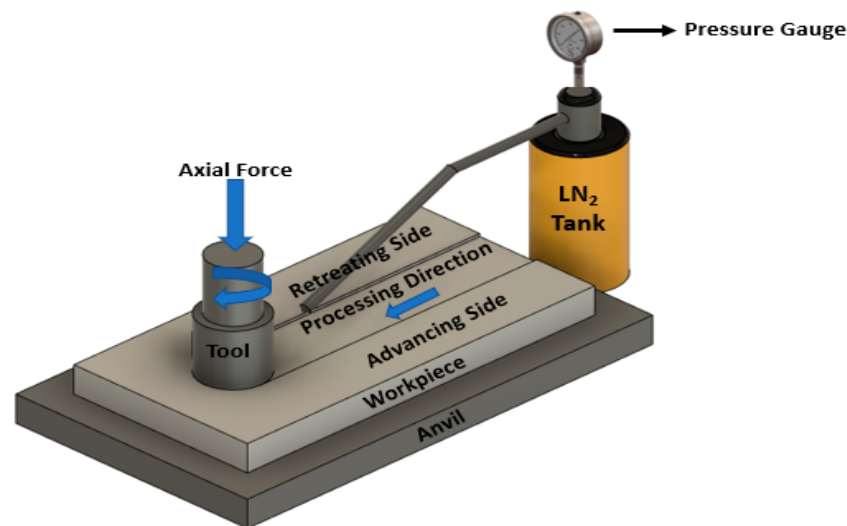


Figure 10. Schematic representation of FSP under LN environment.

Many researchers reported the usage of LN as a cooling medium for improving the performance of the material following FSP. The Al alloy Al5083 subjected to FSP was reported to achieve a suitably high cooling rate the investigators ran FSP with ultrasonic vibration and LN [135]. To evaluate the effectiveness of rapid cooling using LN in an unbiased manner, they performed a comparable test employing standard air cooling. They discovered distinct changes in the microstructure of materials cooled using diverse cooling agents. The key elements of these alterations revolve around the level of fineness in the grain. When the alloy was cooled with LN, approximately three times more grain refinement was observed in the stirring zone compared to a sample cooled with regular air. Furthermore, when compared to standard air-cooling, the use of LN resulted in a consistently enhanced combination of strength and ductility.

The influence of FSP under LN treatment on the behavior of an extruded AZ31B alloy with regard to wear and corrosion was reported [136]. The experimental work utilized rotational speeds of 800, 1000, and 1200 rpm, and the tool feed rate has been kept constant at 60 mm/min. In LN-treated samples, a decreased wear rate was achieved, which is about 20% better than the performance of the BM. The average grain size achieved at 1000 rpm was 1.5 μm , which was the finest when compared to the grain sizes obtained at 800 rpm and 1200 rpm, which were 5.3 μm and 3.1 μm , respectively. The findings demonstrated that a reduction in the rate of corrosion could be attained with such refinement in the grain structure. When the treated region contains fine grains and is free of defects, about

37% more HV was obtained compared to the base alloy as a result of cryogenic cooling. Wang et al., 2016 [137] evaluated the microstructural evolution of pure copper, which was processed with LN cooling. Mixed microstructures consisting of nano/ultrafine grains in pure copper were observed by them. The treated zone consisted mostly of ultrafine grains and more than 30 percent nano-sized grains. The processed material showed enhanced mechanical characteristics with an increase in the yield tensile strength from 80 MPa to 381 MPa after two FSP passes.

The influence of LN treatment on the corrosion behavior of AZ91 alloy following FSP was investigated through an immersion test in an NaCl solution [138]. The findings indicated that the cryogenically treated FSP AZ91 Mg alloy samples exhibit a significantly greater improvement in corrosion resistance when compared to AZ91 alloy samples in their as-received state. The scattering of secondary β phase particles of AZ91 Mg alloy due to rapid cooling with the help of LN was the primary reason for the significant enhancement in the corrosion resistance and mechanical performance. Ultra-fine grains of SAF2507 duplex stainless steels through FSP assisted by LN and ethanol-based cryogenic medium were developed [139]. Due to the significantly reduced maximum temperature and shorter period of elevated temperatures, a dual-phase UFG configuration structure was generated comprising ferrite and austenite grains with an average size of approximately 1 μm . The designed ultra-fine grains dual-phase structure facilitated a 22% increase in YS while retaining a superior elongation of 55% due to its exceptional work hardening capabilities. Grain refines along with an increase in α/γ interfaces were attributed to notable enhancement in the YS. The remarkable increase in the presence of geometrically essential dislocations near the deformation-incompatible α/γ interfaces played a key role in enhancing the work-hardening capability of the processed material. The enhanced combination of strength and ductility was achieved due to the ultra-fast cooling facilitated by LN throughout the process. Moreover, the resultant UFG dual-phase structure contributed to an increase in resistance to corrosion.

In a Cu-0.55 Cr-0.2 Zr alloy produced by cryogenic FSP followed by annealing [140], a microstructure composed of nano-to-ultra-fine grains was developed. The mean grain size was about 110 nm as shown in Figure 11. The developed nanostructured material showed excellent electrical conductivity of 89% IASC with the integration of exceptional ultra-high strength of 840 MPa. Moreover, it displayed excellent thermal and mechanical stability. These remarkable qualities are attributable to the nanoscale chromium particles positioned along the grain boundaries, avoiding the grain interior regions. While undergoing annealing, the mobility and the sliding of grain boundaries during tensile deformation were impeded by nanoscale chromium particles. Meanwhile, these nano-sized precipitates diminished electron scattering, leading to an enhancement in the material's conductivity. Such a technique of modifying the microstructure in order to improve the mechanical characteristics along with the electrical properties of the material might be useful in the fabrication of Cu-Cr-Zr alloy cords and wires on a large scale for industrial use.

The usage of LN as a cooling agent for composite development through FSP is also explored well by researchers. UFG microstructure with a mean grain size lesser than 1 μm was achieved for the Al-Mg alloy using pre-positioned TiO_2 particles through FSP [141]. Enhancing the cooling speed during the FSP significantly enhanced the refinement of the grain structure. The HV tensile strength and elongation of the treated materials increased significantly from 80.1 HV, 232.2 MPa, and 13.4% to 165.1 HV, 279.4 MPa, and 21.5%, respectively, as a consequence of grain refining of the composite. The impact on the fracture mode of annealed Al-Mg sheet by the degree of cooling was negligible, the presence of TiO_2 nanoparticles caused a shift from ductile failure to a combination of ductile and brittle fracture. As the degree of cooling increased, the fraction of cleavage fracture decreased, making the material more ductile. Table 3 gives insights into the investigation of LN as a cooling media for the improvement in mechanical characteristics of the processed alloys/composites.

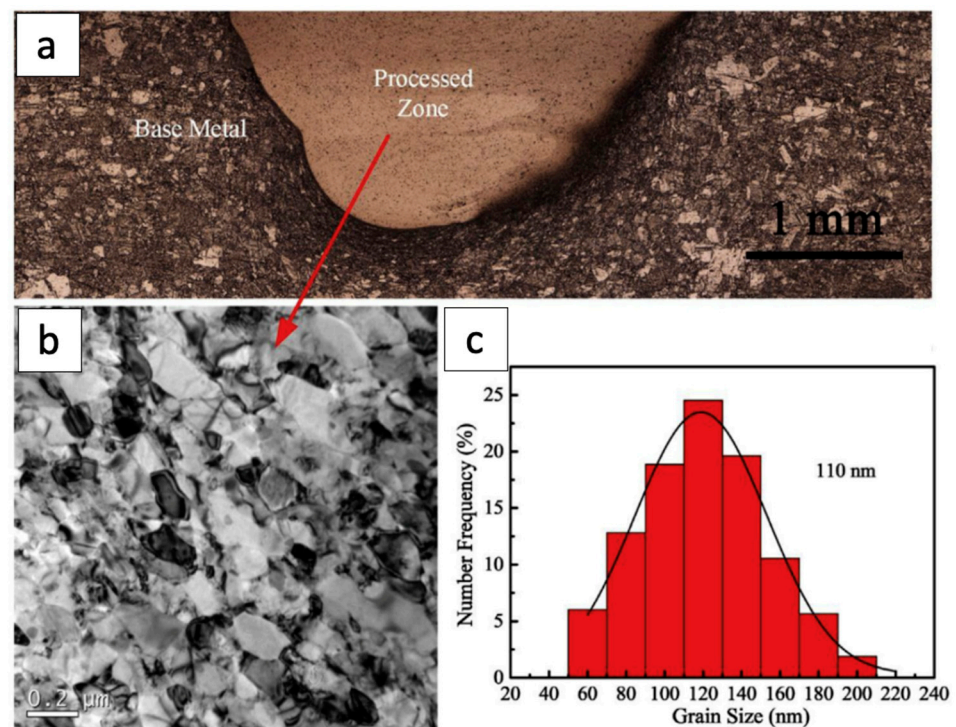


Figure 11. (a) Macrograph of the PZ, (b) microstructure by TEM, (c) grain size distributions of the processed alloy (reprinted with permission from [140]. Copyright © 2019 Elsevier).

Table 3. Meta-analyses on the usage of LN as cooling media in FSP.

Material	Outcomes and Inferences	Ref.
AZ31B	<ul style="list-style-type: none"> -Compared to room temperature samples having a grain size of 8 μm, cryogenic samples showed more uniform grain size of 6 μm and less dispersion. -The thrust force and torque of cryogenic treated samples increased marginally by 5%, this was mainly due to the increased HV of the material because of the rapid cooling mechanism. 	[142]
AZ31B	<ul style="list-style-type: none"> -LN chilling of FSP AZ31B generated smaller average grain size of about 500 nm than those produced at room temperature due to lower heat input. -The majority of the grain formations had high-angle boundaries and displayed prominent textural components. The grains' c-axes were roughly 35–55° distant from the processing direction, indicating significant fiber textures. 	[143]
AZ31B	<ul style="list-style-type: none"> -LN was as a cryogenic coolant in order to reduce the heat input generated during FSP. -Fine grain of 1.92 μm was obtained due to cryogenic FSP an improved strength (YS and UTS), ductility and HV was achieved. Cryogenic FSP produced an axial force of 5600 N when compared to in-air FSP, which produced an axial force of 3800 N. When the axial force is insufficient, there is a decrease in frictional heat production, limiting material flow and leading to defects such as lack of surface fill and wormholes. 	[144]
WE54	<ul style="list-style-type: none"> -As a cooling medium a combination of copper backing plate and LN was used to generate fine equiaxed grains with an average size ranging between 0.8 and 1.3 μm. The mean misorientation was more than 48° and was nearly equal to the Mackenzie random distribution. -When compared to the non-processed material, the YS increased by 10%, from 245 to 270 MPa and ductility values increased 3 to 30%, this was mainly due to rapid cooling during FSP. 	[145]

Table 3. Cont.

Material	Outcomes and Inferences	Ref.
Al-5083	-A combination of LN and methanol was adopted as a cooling medium. -The static recovery and grain advancement that normally occurs inside the treated material as the tool advances was hindered using external cryogenic cooling during FSP. This led to the generation of fine recrystallized grains with a size of 2.14 μm , resulting in a notable enhancement in the HV, tensile strength, and ductility of the alloy after processing.	[146]
Al7075	-This fixture consisted of a rectangular chamber with an empty space beneath the upper surface of the backing plate was fabricated. Copper was used for the fixture's backing plate. In the course of the (FSP, a continuous flow of a chilled combination of LN and methanol was employed to circulate through the empty rectangular chamber of the backing plate. -The material subjected to cryogenic conditions demonstrated a notable grain refinement of 2.4 μm compared to the FSP conducted under non-cryogenic conditions, where the grain refinement was 4.7 μm . Similarly, an effect on mechanical properties was witnessed with an increase in HV, strength, and ductility.	[147]
AA7075-T6	-This experiment resulted in the fabrication UFG (7075-T6) with an average grain size in the range of 17–25 nm, by spraying liquid N_2 on both the upper and bottom sides of the workpiece during the process. -With the development of UFG an increase in HV and mechanical performance was achieved.	[148]
Al7075-SiC	-An indigenous fixture was fabricated that employed LN and methanol as a cooling medium. -Cryogenic FSP successfully modified the distribution of SiC nanoparticles thereby refining the matrix grain size to 2.1 μm , improved particle–matrix interface properties, and eliminated casting defects. When assessed with the as-cast state, these microstructural modifications substantially enhanced strength from 437 MPa to 552 MPa and marginal deterioration in ductility was endorsed.	[149]
Al-1050/SiC	-FSP with SiC nanoparticles resulted in the generation of extremely fine grain structure and the emergence of shear texture in the stir zone, indicating that the DRV, CDRX, and GDRX were the predominant grain formation phenomenon. -FSP in LN results in the formation of a finer grain structure but had no effect on texture components.	[150]

2.4. Heat Sink Cooling

Materials for heat sink applications need a high heat capacity and should possess a great thermal conductivity to absorb more heat without reaching a very high temperature and transfer it to the surrounding environment for efficient cooling [151]. Al, Cu, and steel alloys are the most commonly used heat sink materials. The Cu alloy offers superior thermal conductivity, corrosion resistance, and antibacterial resistance in comparison to Al and steel alloys. Pure copper has about twice the heat conductivity of Al. However, a few drawbacks are it is three times denser than Al, more expensive, and less ductile than Al. The heat sink material must be determined based on the application and the material being processed. A demonstration of FSP with a backing plate is shown in Figure 12.

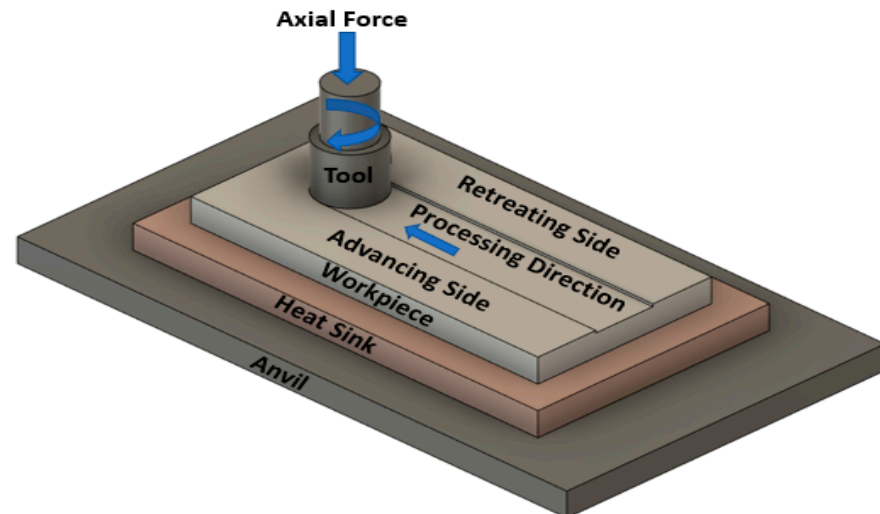


Figure 12. Schematic of FSP utilizing a heat sink.

AZ31B alloy was subjected to FSP using a stationary tool in order to study the grain size at three different zones, using steel and copper plates as a heat sink [152]. For steel as a backing plate, mean grain sizes of 4.98, 4.75, and 4.12 μm were achieved at the top (T), middle (M), and bottom regions (B) of the FSP zone as shown in Figure 13a–c, meanwhile average grain sizes of 4.1, 3.19, and 0.96 μm were obtained at T, M and B zones as indicated in Figure 13d–f, when the Cu plate was used as a heat sink. The Cu backing plate effectively increased the degree of heat conduction at the base, so that heat flows from top to bottom in only one direction. As a result, the rate of grain enlargement diminished rapidly along the heat transfer axis. So, unlike steel backing plates, Cu backing plates generated an interesting microstructural gradient throughout their thickness. Due to the formation of UFG, remarkable improvements in HV and UTS by about 80% and 24% as compared with the BM were achieved.

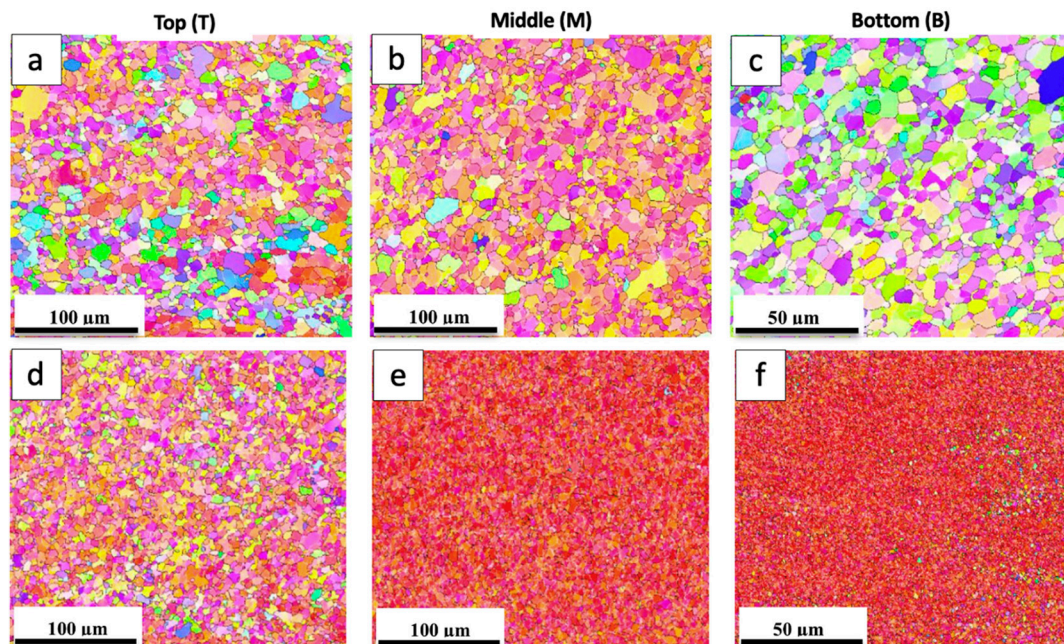


Figure 13. (a–c) EBSD microstructures of AZ31B with steel as backing plate, (d–f) with copper as backing plate (reprinted with permission from [152]. Copyright © 2020 Elsevier).

Low-carbon steel and pure aluminum were processed using FSP in lap configuration [153], where Al is placed at the top with Cu as a backing plate. The prime objective of the researchers was to minimize the intermetallic compound formation through FSP. At rotating speeds greater than 500 rpm, the cladding of low-carbon steel/pure Al with a minimal intermixing layer was effectively accomplished with no discernible flaws or fractures. The backing plate of pure copper considerably reduced the formation of intermetallic compounds at the cladding contact due to the fast cooling of the material.

The AA6063 alloy was investigated with combined effects of tool eccentricity and generated different cooling rates using a Cu backing plate with a constant water flow [154]. Due to the utilization of the auxiliary cooling system during FSP peak temperature dropped from 323.5 to 286 °C, which resulted in excellent grain refinement generating a mean grain size of 8.1 µm while BM had a grain size of 68.3 µm. As a result of this refinement, a tremendous improvement in mechanical performance was witnessed achieving a UTS of 280 MPa with an % of elongation 11.9.

Similarly, the UFG QE22 Mg alloy was developed with an average grain size of 0.63 µm using two FSP passes with the help of active cooling, which included blowing the air on the top of the workpiece area during FSP and a Cu plate as a heat sink [155]. Due to this synergetic cooling strategy, room temperature ductility drastically increased from 7 to 24% without affecting the strength of the alloy and achieved a remarkable formability index of 4680 MPa%. The aforementioned group further investigated the superplastic performance of developed UFG QE22 [156] at various strain rates and reported that they achieved an extraordinary superplasticity of 1630% at 450 °C with a strain rate of $1 \times 10^{-2} \text{ s}^{-1}$.

3. Practical Considerations for Large-Scale Implementation

While a cooling method might be effective in a controlled laboratory environment, scaling it up to an industrial level may present challenges. For instance, LN cooling might be feasible in small-scale experiments but could be logistically complex and costly to implement on a large scale. However, LN cooling has potential applications for developing advanced materials for critical applications due to its excellent cooling performance. In the case of submerged FSP, where a working fluid is involved during the processing, the fluid needs to be replaced frequently to maintain its cooling effectiveness. This makes submerged FSP suitable for macro- and small-scale industries but less practical for large-scale operations due to the high maintenance and material costs. Heat sink cooling is recommended only for specific geometries, as it relies on direct contact between the heat sink and the material being processed. This method lacks scalability because it cannot be easily adapted to various shapes and sizes of workpieces without significant modifications. Air cooling is the best for scalability since it is easy to use and cost-effective. It requires minimal setup and maintenance, making it ideal for large-scale industrial applications. However, while air cooling provides moderate improvement in material performance, it may not achieve the same level of microstructural refinement as more intensive cooling methods. Each cooling method's adaptability to different material types and processing conditions must be considered. Methods that work well for one material may not be as effective for another, especially when scaled up to industrial levels.

4. Conclusions

Fast cooling in FSP is a new and critically important phase in the growth of manufacturing industries. This strategy offers engineers a workflow to customize the microstructure, allowing them to regulate the performance of materials through engineering. By implementing a rapid cooling approach in FSP, the aim is to maintain a minimal temperature for both the processed sample and the tool. This approach positively impacts the work material by enhancing its microstructural refinement while also contributing to prolonged tool lifespan and reduced wear. The homogeneity of the material's structure and the significant reduction in grain size achieved by inhibiting grain growth contribute to the improvement of the mechanical properties of the processed material under fast cooling strategies. The

rate of advancement at which the material cools clearly appears to be affected both by the medium used for cooling and by the technique employed. Because water and cryogenic coolants possess a heat capacity that is far larger than that of air, these coolants can absorb a significant amount of heat. Their use in the most efficient manner subsequently accelerates the pace at which the sample and tool are cooled down and bring down their respective temperatures. In most cases, higher grain refinement may be accomplished when the process is carried out under cryogenic conditions. Achieving an improved material cooling rate is possible through the submerged processing method compared to the use of a heat sink, as the submerged processing technique facilitates a higher rate of heat removal. When evaluating and implementing a cooling method it is important to consider the practicality of a specific approach. This potential arises, among other things, from the feasibility of adapting a given solution under industrial situations in a flawless and cost-effective manner. Table 4 shows the recommended FSP method to be utilized as per the required applications.

Table 4. Recommended FSP method as per required applications.

Cooling	Application	Recommended FSP Method
Air	Suitable for less sensitive materials like medium carbon low alloy steels (e.g., EN8) and Cu alloys where mild cooling is sufficient.	Air jets and forced cooling.
Water	Generally utilized with steel alloys and general purpose Al alloys (e.g., 6061) for automobile parts.	Water spray, immersion cooling.
LN	Used with Mg alloys (AZ91), Al alloys (7075) for aerospace applications requiring high strength and heat resistance.	Direct application during FSP or cryogenic bath.
Heat Sink	Effective for high-thermal-conductivity materials like copper-based HEAs (CuCrFeNiMn) used in electronics cooling.	Fixed heat sinks attached during FSP to control thermal gradients

The introduction of auxiliary cooling systems in FSP presents an aspiring emerging trend that opens up new possibilities for modifying the microstructure and overall performance of the processed materials. In the following years, research will concentrate on technologies that enable even greater material cooling rates during FSP and that can be used in industrial situations without extensive and expensive modification of the machinery. The simplicity, adaptability, and absence of material restrictions of a cooling system will determine its success. With the FSP cooling system in research, pre- and post-treatment of the materials can be minimized. The use of compressed air as a cooling agent, especially when cooled through a cooling jet nozzle, is expected to gain increased popularity as installation and customization of the aforementioned technologies in industrial settings is flexible. Nevertheless, coolants in the FSP process provide novel ways to tailor materials' microstructure and improve their application capabilities.

5. Future Prospects

Adopting multi-physics approaches that not only consider the thermal aspects but also incorporate the mechanical and metallurgical effects should be taken up this holistic understanding would contribute to more accurate predictions and control of the microstructure. Future research could delve deeper into the integration of computational modeling methods, such as finite element analysis or computational fluid dynamics. These models can simulate the complex thermal and mechanical interactions during FSP, aiding in the optimization of cooling strategies for enhanced microstructural control. Exploring unconventional cooling mediums beyond traditional methods could be a future avenue. This might involve investigating the use of advanced liquid coolants, cryogenic cooling, or even innovative approaches like the use of nanofluids to achieve rapid and controlled cooling during FSP. Developing in situ monitoring techniques for real-time assessment of

microstructural evolution during FSP could be a significant advancement. This could be coupled with closed-loop control systems, enabling adjustments to cooling strategies in real time based on the observed microstructural changes. The application of optimization algorithms for determining the most effective cooling strategies based on defined objectives and specific materials, such as achieving specific microstructural characteristics or minimizing energy consumption can be investigated. The environmental implications of different cooling strategies in FSP can be explored by assessing the energy consumption, waste generation, and overall sustainability of various cooling approaches would be essential for the broader adoption of these techniques. Scaling up the findings from laboratory-scale experiments to industrial applications is a crucial focus on addressing challenges related to implementing advanced cooling strategies in large-scale manufacturing processes, considering factors like cost-effectiveness and feasibility.

Author Contributions: M.S.P., R.J.I. and M.F.K. collected the data. A.R., M.F.K. and M.J. conceptualized the study. All authors have read and agreed to the published version of the manuscript.

Funding: The authors confirm that there is no funding to disclose.

Data Availability Statement: The raw data supporting the conclusions of this article will be made available by the authors on request.

Conflicts of Interest: The authors declare no competing interests.

Abbreviations

FSP	Friction stir processing
FSW	Friction stir welding
SZ	Stirred zone
BM	Base metal
FG	Fine grains
LN	Liquid nitrogen
HV	Vickers hardness
YS	Yield strength
UFG	Ultra-fine grains
UTS	Ultimate tensile strength

References

1. Elayaperumal, A.; Arulvel, S.; Manikandan, R. Tribology Characterization of Plasma Sprayed Zirconia-Alumina and Fused Zirconia-Alumina Composite Coated Al-Si Alloy at Different Sliding Velocity and Load Conditions. *Silicon* **2022**, *14*, 4707–4722. [\[CrossRef\]](#)
2. Suvorov, D.V.; Gololobov, G.P.; Tarabrin, D.Y.; Slivkin, E.V.; Karabanov, S.M.; Tolstoguzov, A. Electrochemical deposition of Ni-W crack-free coatings. *Coatings* **2018**, *8*, 233. [\[CrossRef\]](#)
3. Biradar, A.; Kandasamy, J. A novel preparation and characterization of electroless NiP/MWCNT composite coated UHMWPE fabric in terms of wettability, electrical conductivity, thermal stability and breaking load resistance. *Mater. Chem. Phys.* **2023**, *299*, 127486. [\[CrossRef\]](#)
4. Su, J.Q.; Nelson, T.W.; Sterling, C.J. Grain refinement of aluminum alloys by friction stir processing. *Philos. Mag.* **2006**, *86*, 1–24. [\[CrossRef\]](#)
5. McNelley, T.R.; Swaminathan, S.; Su, J.Q. Recrystallization mechanisms during friction stir welding/processing of aluminum alloys. *Scr. Mater.* **2008**, *58*, 349–354. [\[CrossRef\]](#)
6. Heidarzadeh, A.; Mironov, S.; Kaibyshev, R.; Çam, G.; Simar, A.; Gerlich, A.; Khodabakhshi, F.; Mostafaei, A.; Field, D.P.; Robson, J.D.; et al. Friction stir welding/processing of metals and alloys: A comprehensive review on microstructural evolution. *Prog. Mater. Sci.* **2021**, *117*, 100752. [\[CrossRef\]](#)
7. Mishra, R.S.; Ma, Z.Y. Friction stir welding and processing. *Mater. Sci. Eng. R Rep.* **2005**, *50*, 1–78. [\[CrossRef\]](#)
8. Mishra, R.S.; Ma, Z.Y.; Charit, I. Friction stir processing: A novel technique for fabrication of surface composite. *Mater. Sci. Eng. A* **2003**, *341*, 307–310. [\[CrossRef\]](#)
9. Jiang, J.; Jiang, F.; Zhang, M.; Yi, K. Microstructure evolution and tensile property of deformed Al–Mg–Sc alloy: Comparison of ECAP and FSP. *J. Mater. Res. Technol.* **2023**, *22*, 2612–2626. [\[CrossRef\]](#)
10. Papantoniou, I.G.; Markopoulos, A.P.; Manolacos, D.E. A new approach in surface modification and surface hardening of aluminum alloys using friction stir process: Cu-Reinforced AA5083. *Materials* **2020**, *13*, 1278. [\[CrossRef\]](#)

11. Arun Kumar, R.; Aakash Kumar, R.G.; Anees Ahamed, K.; Denise Alstyn, B.; Vignesh, V. Review of friction stir processing of aluminium alloys. *Mater. Today Proc.* **2019**, *16*, 1048–1054. [\[CrossRef\]](#)
12. Prasad, R.; Tewari, S.P.; Singh, J.K. Effect of multi-pass friction stir processing on microstructural, mechanical and tribological behaviour of as-cast Al-Zn-Mg-Cu alloy. *Mater. Res. Express* **2019**, *6*, 096579. [\[CrossRef\]](#)
13. Sun, N.; Apelian, D. Friction Stir Processing of Aluminum Alloy A206: Part I—Microstructure Evolution. *Int. J. Met.* **2019**, *13*, 234–243. [\[CrossRef\]](#)
14. Guru, P.R.; Khan MD, F.; Panigrahi, S.K.; Ram, G.D.J. Enhancing strength, ductility and machinability of a Al-Si cast alloy by friction stir processing. *J. Manuf. Process.* **2015**, *18*, 67–74. [\[CrossRef\]](#)
15. Qin, D.; Shen, H.; Shen, Z.; Chen, H.; Fu, L. Manufacture of biodegradable magnesium alloy by high speed friction stir processing. *J. Manuf. Process.* **2018**, *36*, 22–32. [\[CrossRef\]](#)
16. Nasiri, Z.; Sarkari Khorrami, M.; Mirzadeh, H.; Emamy, M. Enhanced mechanical properties of as-cast Mg-Al-Ca magnesium alloys by friction stir processing. *Mater. Lett.* **2021**, *296*, 129880. [\[CrossRef\]](#)
17. Khan MD, F.; Panigrahi, S.K. Achieving excellent thermal stability and very high activation energy in an ultrafine-grained magnesium silver rare earth alloy prepared by friction stir processing. *Mater. Sci. Eng. A* **2016**, *675*, 338–344. [\[CrossRef\]](#)
18. Basak, A.K.; Pramanik, A.; Prakash, C.; Shankar, S.; Gupta, L.R.; Smirnov, V.A.; Al-Kahtani, A.A. Microstructural and micro-mechanical behaviours of friction stir processed magnesium alloy. *J. Mater. Res. Technol.* **2023**, *25*, 6303–6312. [\[CrossRef\]](#)
19. del Valle, J.A.; Rey, P.; Gesto, D.; Verdera, D.; Jiménez, J.A.; Ruano, O.A. Mechanical properties of ultra-fine grained AZ91 magnesium alloy processed by friction stir processing. *Mater. Sci. Eng. A* **2015**, *628*, 198–206. [\[CrossRef\]](#)
20. Iranshahi, F.; Nasiri, M.B.; Warchomicka, F.G.; Sommitsch, C. Investigation of the degradation rate of electron beam processed and friction stir processed biocompatible ZKX50 magnesium alloy. *J. Magnes. Alloys* **2022**, *10*, 707–720. [\[CrossRef\]](#)
21. Balachandran, S.; Mishra, R.S.; Banerjee, D. Friction stir processing of a metastable β titanium alloy in β and $\alpha + \beta$ phase fields. *Mater. Sci. Eng. A* **2020**, *772*, 138705. [\[CrossRef\]](#)
22. Jiang, L.; Huang, W.; Liu, C.; Chai, L.; Yang, X.; Xu, Q. Microstructure, texture evolution and mechanical properties of pure Ti by friction stir processing with slow rotation speed. *Mater. Charact.* **2019**, *148*, 1–8. [\[CrossRef\]](#)
23. Vakili-Azghandi, M.; Roknian, M.; Szpunar, J.A.; Mousavizade, S.M. Surface modification of pure titanium via friction stir processing: Microstructure evolution and dry sliding wear performance. *J. Alloys Compd.* **2020**, *816*, 152557. [\[CrossRef\]](#)
24. Zhang, W.; Ding, H.; Cai, M.; Yang, W.; Li, J. Low-temperature superplastic deformation mechanism in Ti-6Al-4V alloy processed by friction stir processing. *Mater. Sci. Eng. A* **2019**, *764*, 138261. [\[CrossRef\]](#)
25. Zhang, W.; Ding, H.; Cai, M.; Yang, W.; Li, J. Ultra-grain refinement and enhanced low-temperature superplasticity in a friction stir-processed Ti-6Al-4V alloy. *Mater. Sci. Eng. A* **2018**, *727*, 90–96. [\[CrossRef\]](#)
26. Cartigueyen, S.; Mahadevan, K. Study of friction stir processed zone under different tool pin profiles in pure copper. *IOSR J. Mech. Civ. Eng.* **2014**, *11*, 06–12. [\[CrossRef\]](#)
27. Bheekya Naik, R.; Venkateswara Reddy, K.; Madhusudhan Reddy, G.; Arockia Kumar, R. Development of High-Strength and High-Electrical Conductivity Cu-Zr Alloy through Friction Stir Processing. *Trans. Indian Inst. Met.* **2019**, *72*, 1431–1435. [\[CrossRef\]](#)
28. Dehghani, K.; Mazinani, M. Forming nanocrystalline surface layers in copper using friction stir processing. *Mater. Manuf. Process.* **2011**, *26*, 922–925. [\[CrossRef\]](#)
29. Shamsipur, A.; Asadkarami, S. Microstructure and mechanical properties of copper surface composite layers reinforced by nano and microscale SiC particles via friction stir processing. *Adv. Compos. Mater.* **2019**, *28*, 591–606. [\[CrossRef\]](#)
30. Thankachan, T.; Prakash, K.S.; Kavimani, V. Investigations on the effect of friction stir processing on Cu-BN surface composites. *Mater. Manuf. Process.* **2018**, *33*, 299–307. [\[CrossRef\]](#)
31. Langlade, C.; Roman, A.; Schlegel, D.; Gete, E.; Folea, M. Formation of a Tribologically Transformed Surface (TTS) on AISI 1045 Steel by Friction Stir Processing. *Mater. Manuf. Process.* **2016**, *31*, 1565–1572. [\[CrossRef\]](#)
32. Sekban, D.M.; Aktarer, S.M.; Yanar, H.; Alsaran, A.; Purcek, G. Improvement the wear behavior of low carbon steels by friction stir processing. *IOP Conf. Ser. Mater. Sci. Eng.* **2017**, *174*, 012058. [\[CrossRef\]](#)
33. Ralls, A.M.; Daroonparvar, M.; Kasar, A.K.; Misra, M.; Menezes, P.L. Influence of Friction Stir Processing on the Friction, Wear and Corrosion Mechanisms of Solid-State Additively Manufactured 316L Duplex Stainless Steel. *Tribol. Int.* **2023**, *178*, 108033. [\[CrossRef\]](#)
34. Chen, Y.C.; Fujii, H.; Tsumura, T.; Kitagawa, Y.; Nakata, K.; Ikeuchi, K.; Matsubayashi, K.; Michishita, Y.; Fujiya, Y.; Katoh, J. Friction stir processing of 316L stainless steel plate. *Sci. Technol. Weld. Join.* **2009**, *14*, 197–201. [\[CrossRef\]](#)
35. Eskandari, F.; Atapour, M.; Golozar, M.A.; Sadeghi, B.; Cavaliere, P. The microstructure and wear behaviour of friction stir processed AISI 430 ferritic stainless steel. *Tribol.-Mater. Surfaces Interfaces* **2019**, *13*, 172–181. [\[CrossRef\]](#)
36. Ji, X.; Cui, L.; Wang, D.; Li, H.; Liu, Y.; Zhang, C.; Gao, H. Microstructure and high-temperature mechanical properties of RAFM steel processed by friction stir processing combined with tempering heat treatment. *Mater. Sci. Eng. A* **2022**, *831*, 142195. [\[CrossRef\]](#)
37. Yugandhar, M.; Mothilal, M.; Manjunatha, B.; Kannan, T.D.; Patel, M.S.; Nallusamy, S. RS/AS and Nugget Zone SEM Analysis and Mathematical Equations for Parameter Optimization on Friction Stir Welding Tool. *Int. J. Veh. Struct. Syst.* **2023**, *15*, 439–445. [\[CrossRef\]](#)
38. Li, K.; Liu, X.; Zhao, Y. Research status and prospect of friction stir processing technology. *Coatings* **2019**, *9*, 129. [\[CrossRef\]](#)

39. Patel, V.; Li, W.; Xu, Y. Stationary shoulder tool in friction stir processing: A novel low heat input tooling system for magnesium alloy. *Mater. Manuf. Process.* **2019**, *34*, 177–182. [\[CrossRef\]](#)
40. Wenjing, Y.; Hua, D.; Jizhong, L. Parametric optimization for friction stir processing in Al-Zn-Mg-Cu alloy. *Mater. Manuf. Process.* **2022**, *37*, 1–10. [\[CrossRef\]](#)
41. Chai, F.; Zhang, D.T.; Li, Y.Y. Effect of rotation speeds on microstructures and tensile properties of submerged friction stir processed AZ31 magnesium alloy. *Mater. Res. Innov.* **2014**, *18*, 4152–4156. [\[CrossRef\]](#)
42. Yang, X.; Dong, P.; Yan, Z.; Cheng, B.; Zhai, X.; Chen, H.; Zhang, H.; Wang, W. AlCoCrFeNi high-entropy alloy particle reinforced 5083Al matrix composites with fine grain structure fabricated by submerged friction stir processing. *J. Alloys Compd.* **2020**, *836*, 155411. [\[CrossRef\]](#)
43. Patel, M.; Rahaman, A.; Immanuel, R.J. Tribological profiling of Mg-Gd-Y Alloy: Investigating sliding wear dynamics under varied temperature conditions. *Mater. Lett.* **2024**, *370*, 136808. [\[CrossRef\]](#)
44. Yang, X.; Zhang, H.; Cheng, B.; Liu, Y.; Yan, Z.; Dong, P.; Wang, W. Microstructural, Microhardness and tribological analysis of cooling-assisted friction stir processing of high-entropy alloy particles reinforced aluminum alloy surface composites. *Surf. Topogr. Metrol. Prop.* **2020**, *8*, 035012. [\[CrossRef\]](#)
45. Zhang, H.; Xue, P.; Wang, D.; Wu, L.H.; Ni, D.R.; Xiao, B.L.; Ma, Z.Y. A novel approach to achieve high yield strength high nitrogen stainless steel with superior ductility and corrosion resistance. *Mater. Lett.* **2019**, *242*, 91–94. [\[CrossRef\]](#)
46. Keerthana, B.V.S.; Satyanarayana, M.V.N.V.; Reddy, K.V.; Shankar, M.N.S. Effect of post-process and in-process cooling on wide-area stir zone processed via friction stir processing with pin overlapping. *Eng. Res. Express* **2023**, *5*, 025060. [\[CrossRef\]](#)
47. Mirzadeh, H. High strain rate superplasticity via friction stir processing (FSP): A review. *Mater. Sci. Eng. A* **2021**, *819*, 141499. [\[CrossRef\]](#)
48. Mohamadigangaraj, J.; Nourouzi, S.; Aval, H.J. The effect of heat treatment and cooling conditions on friction stir processing of A390-10 wt% SiC aluminium matrix composite. *Mater. Chem. Phys.* **2020**, *263*, 124423. [\[CrossRef\]](#)
49. Patel, M.S.; Besekar, A.; Annamalai, S.; Kumar, M.S.; Jain, R.; Immanuel, R.J. Role of Nickel Particulate Reinforcement on Microstructure and Mechanical Performance of AZ31 Magnesium Composite. *Trans. Indian Inst. Met.* **2024**. [\[CrossRef\]](#)
50. Patel, V.; Li, W.; Vairis, A.; Badheka, V. Recent Development in Friction Stir Processing as a Solid-State Grain Refinement Technique: Microstructural Evolution and Property Enhancement. *Crit. Rev. Solid State Mater. Sci.* **2019**, *44*, 378–426. [\[CrossRef\]](#)
51. Chen, J.; Li, Z.; Han, J.; Peng, L.; Fujii, H.; Wu, Y.; Cheng, H. Investigation on microstructure evolution of Mg-Gd-Zn-Zr alloys during friction stir processing by liquid CO₂ cooling assisted stop action. *Mater. Sci. Eng. A* **2023**, *876*, 145140. [\[CrossRef\]](#)
52. Patel, V.V.; Badheka, V.J.; Patel, U.; Patel, S.; Patel, S.; Zala, S.; Badheka, K. Experimental Investigation on Hybrid Friction Stir Processing using compressed air in Aluminum 7075 alloy. *Mater. Today Proc.* **2017**, *4*, 10025–10029. [\[CrossRef\]](#)
53. Snyder, B.; Strauss, A.M. In-process cooling of friction stir extruded joints for increased weld performance via compressed air, water, granulated dry ice, and liquid nitrogen. *J. Manuf. Process.* **2021**, *68*, 1004–1017. [\[CrossRef\]](#)
54. Xu, N.; Ueji, R.; Morisada, Y.; Fujii, H. Modification of mechanical properties of friction stir welded Cu joint by additional liquid CO₂ cooling. *Mater. Des.* **2014**, *56*, 20–25. [\[CrossRef\]](#)
55. Wang, J.; Yang, K.; Zhang, Y.; Lu, Y.L.; Bai, Z.H.; Li, X.C. Investigation on variations of microstructures and mechanical properties along thickness direction of friction stir processed AA2014 aluminum alloy via ultra-rapid cooling. *Mater. Charact.* **2021**, *179*, 111352. [\[CrossRef\]](#)
56. Xue, P.; Wang, B.B.; Chen, F.F.; Wang, W.G.; Xiao, B.L.; Ma, Z.Y. Microstructure and mechanical properties of friction stir processed Cu with an ideal ultrafine-grained structure. *Mater. Charact.* **2016**, *121*, 187–194. [\[CrossRef\]](#)
57. Moaref, A.; Rabiezadeh, A. Microstructural evaluation and tribological properties of underwater friction stir processed CP-copper and its alloy. *Trans. Nonferrous Met. Soc. China (Engl. Ed.)* **2020**, *30*, 972–981. [\[CrossRef\]](#)
58. Bansal, A.; Singla, A.K.; Dwivedi, V.; Goyal, D.K.; Singla, J.; Gupta, M.K.; Krolczyk, G.M. Influence of cryogenic treatment on mechanical performance of friction stir Al-Zn-Cu alloy weldments. *J. Manuf. Process.* **2020**, *56*, 43–53. [\[CrossRef\]](#)
59. Xu, N.; Bao, Y. Enhanced mechanical properties of tungsten inert gas welded AZ31 magnesium alloy joint using two-pass friction stir processing with rapid cooling. *Mater. Sci. Eng. A* **2016**, *655*, 292–299. [\[CrossRef\]](#)
60. Raja, S.; Yusof, F.; bin Muhamad, R.; Jamaludin, M.F.; Khan, M.F.; Shaikh, M.B.N.; Arif, S.; Alam, M.A. *Surface Modification of Mg Alloys: An Insight into Friction Stir-Based Techniques*; CRC Press: Boca Raton, FL, USA, 2024; ISBN 9780128140635.
61. Amirov, A.; Eliseev, A.; Beloborodov, V. Wear of Ni-Based Superalloy Tools in Friction Stir Processing of Commercially Pure Titanium. *Lubricants* **2023**, *11*, 307. [\[CrossRef\]](#)
62. Liu, F.C.; Ma, Z.Y. Low-temperature superplasticity of friction stir processed Al-Zn-Mg-Cu alloy. *Scr. Mater.* **2008**, *58*, 667–670. [\[CrossRef\]](#)
63. Fydrych, D.; Tomków, J. Underwater Processing of Materials. *Materials* **2022**, *15*, 4902. [\[CrossRef\]](#) [\[PubMed\]](#)
64. Heidarian, M.; Mostafapoor, S. Microstructure and Mechanical Properties of Friction Stir Processed AISI 316 Stainless Steel: Evaluation of the Effect of Cooling Media and Multi-Step Processing on Microstructure and Mechanical Properties of Friction Stir Processed AISI 316 Stainless Ste. *Metallogr. Microstruct. Anal.* **2022**, *11*, 72–87. [\[CrossRef\]](#)
65. Mazaheri, H.; Aval, H.J.; Jamaati, R. Manufacturing of Ultrafine-Grained Copper via Rolling and Cooling-Assisted Friction Stir Processing: Effect of Traverse Speed. *J. Mater. Eng. Perform.* **2023**, *32*, 3780–3795. [\[CrossRef\]](#)

66. Asadi, P.; Besharati Givi, M.K.; Parvin, N.; Araei, A.; Taherishargh, M.; Tutunchilar, S. On the role of cooling and tool rotational direction on microstructure and mechanical properties of friction stir processed AZ91. *Int. J. Adv. Manuf. Technol.* **2012**, *63*, 987–997. [\[CrossRef\]](#)
67. Satyanarayana, M.V.N.V.; Manohar, G.; Jain, V.K.S.; Kumar, K.K.; Kumar, A.; Sundar, S. Influence of Cooling Media on the Electrochemical Behavior of Friction Stir Processed Al2014 Alloy. *JOM* **2023**, *75*, 526–536. [\[CrossRef\]](#)
68. Arora, H.S.; Singh, H.; Dhindaw, B.K. Some observations on microstructural changes in a Mg-based AE42 alloy subjected to friction stir processing. *Metall. Mater. Trans. B Process Metall. Mater. Process. Sci.* **2012**, *43*, 92–108. [\[CrossRef\]](#)
69. Liu, W.; Yan, Y.; Sun, T.; Wu, S.; Shen, Y. Influence of cooling water temperature on ME20M magnesium alloy submerged friction stir welding: A numerical and experimental study. *Int. J. Adv. Manuf. Technol.* **2019**, *105*, 5203–5215. [\[CrossRef\]](#)
70. Wu, J.; Cao, F.J.; Sun, T.; Huang, G.Q.; Li, M.S.; Hou, W.T.; Piao, Z.Y.; Shen, Z.K.; Shen, Y.F. Developing ultrafine-grained structure with balanced α/γ fraction via underwater friction stir processing enables enhanced wear and corrosion resistance of duplex stainless steel. *Surf. Coat. Technol.* **2023**, *457*, 129295. [\[CrossRef\]](#)
71. Subramani, V.; Jayavel, B.; Sengottuvelu, R.; Lazar, P.J.L. Assessment of microstructure and mechanical properties of stir zone seam of friction stir welded magnesium AZ31B through Nano-SiC. *Materials* **2019**, *12*, 1044. [\[CrossRef\]](#)
72. Orozco-Caballero, A.; Cepeda-Jiménez, C.M.; Hidalgo-Manrique, P.; Rey, P.; Gesto, D.; Verdera, D.; Ruano, O.A.; Carreño, F. Lowering the temperature for high strain rate superplasticity in an Al-Mg-Zn-Cu alloy via cooled friction stir processing. *Mater. Chem. Phys.* **2013**, *142*, 182–185. [\[CrossRef\]](#)
73. Hui, W.; Zhang, Y.; Shao, C.; Chen, S.; Zhao, X.; Dong, H. Enhancing the Mechanical Properties of Vanadium-Microalloyed Medium-Carbon Steel by Optimizing Post-Forging Cooling Conditions. *Mater. Manuf. Process.* **2016**, *31*, 770–775. [\[CrossRef\]](#)
74. Patel, V.; Badheka, V.; Li, W.; Akkiredy, S. Hybrid friction stir processing with active cooling approach to enhance superplastic behavior of AA7075 aluminum alloy. *Arch. Civ. Mech. Eng.* **2019**, *19*, 1368–1380. [\[CrossRef\]](#)
75. Akbari, M.; Khalkhali, A.; Keshavarz, S.M.E.; Sarikhani, E. The effect of in-process cooling conditions on temperature, force, wear resistance, microstructural, and mechanical properties of friction stir processed A356. *Proc. Inst. Mech. Eng. Part L J. Mater. Des. Appl.* **2018**, *232*, 429–437. [\[CrossRef\]](#)
76. Iwaszko, J.; Kudła, K. Evolution of Microstructure and Properties of Air-Cooled Friction-Stir-Processed 7075 Aluminum Alloy. *Materials* **2022**, *15*, 2633. [\[CrossRef\]](#)
77. Iwaszko, J.; Kud, K. Microstructure, hardness, and wear resistance of AZ91 magnesium alloy produced by friction stir processing with air-cooling. *Int. J. Adv. Manuf. Technol.* **2021**, *116*, 1309–1323. [\[CrossRef\]](#)
78. El-Mahallawy, N.; Majed, A.; Maboud, A.A.G.A. Effect of FSP process parameters with air blowing on microstructure and hardness of NiAl Bronze alloy. *Mater. Res. Express* **2020**, *7*, 016590. [\[CrossRef\]](#)
79. Almousa, N.H.; Alotaibi, M.R.; Alsohybani, M.; Radziszewski, D.; Alnoman, S.M.; Alotaibi, B.M.; Khayyat, M.M. Paraffin Wax [As a Phase Changing Material (PCM)] Based Composites Containing Multi-Walled Carbon Nanotubes for Thermal Energy Storage (TES) Development. *Crystals* **2021**, *11*, 951. [\[CrossRef\]](#)
80. Sipova, M.; Marusakova, D.; Aparicio, C.; Prochazka, J.; Halodova, P. A study on the corrosion behaviour of stainless steel 08Cr18Ni10Ti in supercritical water. *Corros. Sci.* **2023**, *211*, 110853. [\[CrossRef\]](#)
81. Huang, H.; Yang, W. Corrosion behavior of AZ91D magnesium alloy in distilled water. *Arab. J. Chem.* **2020**, *13*, 6044–6055. [\[CrossRef\]](#)
82. Huang, L.; Wang, K.; Wang, W.; Yuan, J.; Qiao, K.; Yang, T.; Peng, P.; Li, T. Effects of grain size and texture on stress corrosion cracking of friction stir processed AZ80 magnesium alloy. *Eng. Fail. Anal.* **2018**, *92*, 392–404. [\[CrossRef\]](#)
83. Satyanarayana, M.V.N.V.; Bathula, S.; Kumar, A. Effect of external cooling on fatigue crack growth behaviour of friction stir processed AA6061 alloy. *Eng. Fract. Mech.* **2022**, *261*, 108236. [\[CrossRef\]](#)
84. Pettinari-Sturmelt, F.; Jouiad, M.; Kirchner, H.O.K.; Clement, N.; Coujou, A. Local disordering and reordering phenomena induced by mobile dislocations in short-range-ordered solid solutions. *Philos. Mag. A Phys. Condens. Matter Struct. Defects Mech. Prop.* **2002**, *82*, 3045–3054. [\[CrossRef\]](#)
85. Keerthana, B.V.S.; Satyanarayana, M.V.N.V.; Shankar, M.N.S. Effect of Cooling-Assisted Friction Stir Processing on Corrosion Behavior of AA5083 Alloy. *J. Inst. Eng. Ser. D* **2023**, *105*, 191–200. [\[CrossRef\]](#)
86. Heidarpour, A.; Ahmadi, S.; Rohani, N. FSP Pass Number and Cooling Effects on the Microstructure and Properties of AZ31. *J. Adv. Mater. Process.* **2018**, *6*, 47–58.
87. Ramaian, S.; Santhanam, S.K.V.; Muthuguru, P. Effect of scroll pin profile and tool rotational speed on mechanical properties of submerged friction stir processed AZ31B magnesium alloy. *Mater. Res.* **2018**, *21*, e20170769. [\[CrossRef\]](#)
88. Luo, X.; Liu, H.; Kang, L.; Lin, J.; Zhang, D.; Li, D.; Chen, D. Achieving Superior Superplasticity in a Mg–6Al–Zn Plate via Multi-pass Submerged Friction Stir Processing. *Acta Metall. Sin. (Engl. Lett.)* **2022**, *35*, 757–762. [\[CrossRef\]](#)
89. Zhang, D.; Chai, F.; Li, Y. High strain rate superplasticity of a fine-grained AZ91 magnesium alloy prepared by friction stir processing. In Proceedings of the 8th Pacific Rim International Congress on Advanced Materials and Processing, Waikoloa, HI, USA, 4–9 August 2013; Volume 2, pp. 1065–1071. [\[CrossRef\]](#)
90. Arora, H.S.; Ayyagari, A.; Saini, J.; Selvam, K.; Riyadh, S.; Pole, M.; Grewal, H.S.; Mukherjee, S. High Tensile Ductility and Strength in Dual-phase Bimodal Steel through Stationary Friction Stir Processing. *Sci. Rep.* **2019**, *9*, 1972. [\[CrossRef\]](#)
91. Xue, P.; Xiao, B.L.; Ma, Z.Y. Achieving ultrafine-grained structure in a pure nickel by friction stir processing with additional cooling. *Mater. Des.* **2014**, *56*, 848–851. [\[CrossRef\]](#)

92. Huang, L.Y.; Wang, K.S.; Wang, W.; Zhao, K.; Yuan, J.; Qiao, K.; Zhang, B.; Cai, J. Mechanical and corrosion properties of low-carbon steel prepared by friction stir processing. *Int. J. Miner. Metall. Mater.* **2019**, *26*, 202–209. [\[CrossRef\]](#)
93. Heidarzadeh, A.; Mohammadzadeh, R. Developing α/β Laminar Composite Structure in CuZn Alloy by Heat Treatment and Submerged Friction Stir Processing. *Iran. J. Mater. Form.* **2021**, *8*, 26–32.
94. Bharti, S.; Ghetiya, N.D.; Patel, K.M. A review on manufacturing the surface composites by friction stir processing. *Mater. Manuf. Process.* **2021**, *36*, 135–170. [\[CrossRef\]](#)
95. Huang, G.Q.; Yan, Y.F.; Wu, J.; Shen, Y.F.; Gerlich, A.P. Microstructure and mechanical properties of fine-grained aluminum matrix composite reinforced with nitinol shape memory alloy particulates produced by underwater friction stir processing. *J. Alloys Compd.* **2019**, *786*, 257–271. [\[CrossRef\]](#)
96. Srivastava, M.; Rathee, S.; Maheshwari, S.; Siddiquee, A.N. Influence of multiple-passes on microstructure and mechanical properties of Al-Mg/SiC surface composites fabricated via underwater friction stir processing. *Mater. Res. Express* **2018**, *5*, 066511. [\[CrossRef\]](#)
97. Gao, J.; Shen, Y.; Li, C. Fabrication of high-density polyethylene/multiwalled carbon nanotube composites via submerged friction stir processing. *J. Thermoplast. Compos. Mater.* **2017**, *30*, 241–254. [\[CrossRef\]](#)
98. Manroo, S.A.; Khan, N.Z.; Ahmad, B. Study on surface modification and fabrication of surface composites of magnesium alloys by friction stir processing: A review. *J. Eng. Appl. Sci.* **2022**, *69*, 25. [\[CrossRef\]](#)
99. Yang, X.; Yan, Z.; Dong, P.; Cheng, B.; Zhang, J.; Zhang, T.; Zhang, H.; Wang, W. Surface modification of aluminum alloy by incorporation of AlCoCrFeNi high entropy alloy particles via underwater friction stir processing. *Surf. Coat. Technol.* **2020**, *385*, 125438. [\[CrossRef\]](#)
100. Huang, L.Y.; Wang, K.; Wang, W.; Zhao, K.; Yuan, J.; Wang, Q.; Qiao, K.; Cai, J. Corrosion properties of low carbon steel prepared by submerged friction stir processing. *Mater. Corros.* **2018**, *69*, 1077–1083. [\[CrossRef\]](#)
101. Selvam, K.; Ayyagari, A.; Grewal, H.S.; Mukherjee, S.; Arora, H.S. Enhancing the erosion-corrosion resistance of steel through friction stir processing. *Wear* **2017**, *386–387*, 129–138. [\[CrossRef\]](#)
102. Satish Kumar, T.; Thankachan, T. Friction stir processing based surface modification of AZ31 magnesium alloy. *Mater. Manuf. Process.* **2023**, *38*, 1426–1435. [\[CrossRef\]](#)
103. Naser, A.Z.; Darras, B.M. Experimental investigation of Mg/SiC composite fabrication via friction stir processing. *Int. J. Adv. Manuf. Technol.* **2017**, *91*, 781–790. [\[CrossRef\]](#)
104. Bourkhani, R.D.; Eivani, A.R.; Nateghi, H.R. Through-thickness inhomogeneity in microstructure and tensile properties and tribological performance of friction stir processed AA1050-Al₂O₃ nanocomposite. *Compos. Part B Eng.* **2019**, *174*, 107061. [\[CrossRef\]](#)
105. Deore, H.A.; Mishra, J.; Rao, A.G.; Bhanushali, B.D.; Hiwarkar, V.D. Utilizing Additive Friction Stir Processing to Fabricate B4C Reinforced Ti-6Al-4V Matrix Surface Composite: Microstructure Refinement and Enhancement in Mechanical Properties. *Met. Mater. Int.* **2022**, *28*, 322–335. [\[CrossRef\]](#)
106. Thankachan, T.; Prakash, K.S.; Kavimani, V. Effect of friction stir processing and hybrid reinforcements on copper. *Mater. Manuf. Process.* **2018**, *33*, 1681–1692. [\[CrossRef\]](#)
107. Murugarajan, A.; Srimath, N. Effect of titanium carbide reinforcement on micro structure and wear properties of annealed AA6082 by friction stir processing. *Adv. Mater. Process. Technol.* **2022**, *8*, 223–230. [\[CrossRef\]](#)
108. Kumar, K.A.; Natarajan, S.; Duraiselvam, M.; Ramachandra, S. Synthesis, characterization and mechanical behavior of Al 3003-TiO₂ surface composites through friction stir processing. *Mater. Manuf. Process.* **2019**, *34*, 183–191. [\[CrossRef\]](#)
109. Teo, G.S.; Liew, K.W.; Kok, C.K. A Study on Friction Stir Processing Parameters of Recycled AA 6063/TiO₂ Surface Composites for Better Tribological Performance. *Metals* **2022**, *12*, 973. [\[CrossRef\]](#)
110. Rao, D.S.; Ramanaiah, N. Process parameters optimization for producing AA6061/TiB₂ composites by friction stir processing. *Stroj. Cas.* **2017**, *67*, 101–117. [\[CrossRef\]](#)
111. Prabhakara, G.V.N.B.; Kumarb, Y.V.R.S.N.P.; Kumarb, P.D.; Kumarb, B.P.; Rajub, M.G.; Naseemab, S.; Kumarc, N.R.; Jagannathamd, M.; Sunile, B.R. Producing Al5083-CNT composites by friction stir processing: Influence of grain refinement and CNT on mechanical and corrosion properties. *Mater. Today Proc.* **2019**, *15*, 44–49. [\[CrossRef\]](#)
112. Saikrishna, N.; Reddy, G.P.K.; Munirathinam, B.; Dumpala, R.; Jagannatham, M.; Sunil, B.R. An investigation on the hardness and corrosion behavior of MWCNT/Mg composites and grain refined Mg. *J. Magnes. Alloys* **2018**, *6*, 83–89. [\[CrossRef\]](#)
113. Huang, G.; Wu, J.; Hou, W.; Shen, Y.; Gao, J. Producing of Al-WC surface composite by additive friction stir processing. *Mater. Manuf. Process.* **2019**, *34*, 147–158. [\[CrossRef\]](#)
114. Bajakke, P.A.; Malik, V.R.; Deshpande, A.S. Particulate metal matrix composites and their fabrication via friction stir processing—A review. *Mater. Manuf. Process.* **2019**, *34*, 833–881. [\[CrossRef\]](#)
115. Mukherjee, M.; Mukherjee, R.; Rahul, A.; Das, D.; Datta, S. Evaluation of Ca-alloyed and HAP-reinforced magnesium matrix surface composite properties developed by friction stir processing. *Mater. Manuf. Process.* **2023**, *39*, 778–786. [\[CrossRef\]](#)
116. Rathinasuriyan, C.; Mystica, A.; Sankar, R.; Senthil Kumar, V.S. Experimental investigation of cooling medium on submerged friction stir processed AZ31 magnesium alloy. *Mater. Today Proc.* **2020**, *46*, 3386–3391. [\[CrossRef\]](#)
117. Sun, T.; Cao, F.; Hu, J.; Shen, Y.; Qu, X.; Xu, W. Developing Ultrafine Twinned Microstructure Enabled Excellent Strength–Ductility Synergy in Mg–Al–Zn Alloy by Submerged Friction Stir Processing. *Metall. Mater. Trans. A Phys. Metall. Mater. Sci.* **2023**, *54*, 4779–4795. [\[CrossRef\]](#)

118. Luo, X.; Cao, G.; Zhang, W.; Qiu, C.; Zhang, D. Ductility improvement of an AZ61 magnesium alloy through two-pass submerged friction stir processing. *Materials* **2017**, *10*, 253. [\[CrossRef\]](#)
119. Luo, X.; Zhang, D.; Zhang, W.; Qiu, C. *Effect of Multi-Pass Submerged Friction Stir Processing on Microstructure Evolution and Mechanical Properties of AZ61 Magnesium Plate*; Advances in Materials Processing. CMC 2017. Lecture Notes in Mechanical Engineering; Springer: Singapore, 2018; Volume 32, ISBN 9789811301070.
120. Chai, F.; Zhang, D.; Li, Y. Microstructures and tensile properties of submerged friction stir processed AZ91 magnesium alloy. *J. Magnes. Alloys* **2015**, *3*, 203–209. [\[CrossRef\]](#)
121. Chai, F.; Zhang, D.; Li, Y.; Zhang, W. Microstructure evolution and mechanical properties of a submerged friction-stir-processed AZ91 magnesium alloy. *J. Mater. Sci.* **2015**, *50*, 3212–3225. [\[CrossRef\]](#)
122. Li, Y.; Guan, Y.; Liu, Y.; Zhai, J.; Hu, K.; Lin, J. Microstructure and tensile properties of the friction stir processed LA103Z alloy. *Mater. Charact.* **2023**, *196*, 112616. [\[CrossRef\]](#)
123. Peng, Y.; Zhang, Q.; Wen, L.; Xie, Z.; Huang, B.; Hu, S.; Tang, H.; Wei, C. An Investigation into Microstructures and Mechanical Properties of 1060 Pure Aluminum during Submerged Friction Stir Processing at a High Rotating Speed. *Metals* **2022**, *12*, 201. [\[CrossRef\]](#)
124. Chen, Y.; Jiang, Y.; Ding, H.; Zhao, J.; Li, J. Effects of friction-stir processing with water cooling on the properties of an Al–Zn–Mg–Cu Alloy. *Mater. Sci. Technol.* **2018**, *34*, 153–160. [\[CrossRef\]](#)
125. Huang, G.; Wu, J.; Hou, W.; Shen, Y. Microstructure, mechanical properties and strengthening mechanism of titanium particle reinforced aluminum matrix composites produced by submerged friction stir processing. *Mater. Sci. Eng. A* **2018**, *734*, 353–363. [\[CrossRef\]](#)
126. Ai, X.; Yue, Y. Microstructure and Mechanical Properties of Friction Stir Processed A356 Cast Al under Air Cooling and Water Cooling. *High Temp. Mater. Proc.* **2017**, *37*, 693–699. [\[CrossRef\]](#)
127. Wang, J.; Lu, Y.; Zhou, D.; Zhang, Y.; Bai, Z.; Li, X. Effects of cooling condition on microstructural evolution and mechanical properties of friction stir processed 2A14 aluminum alloy. *Mater. Res. Express* **2019**, *6*, 126577. [\[CrossRef\]](#)
128. Chen, Y.; Jiang, Y.; Zhang, F.; Ding, H.; Zhao, J.; Ren, Z. Water Cooling Effects on the Microstructural Evolution and Mechanical Properties of Friction-Stir-Processed Al-6061 Alloy. *Trans. Indian Inst. Met.* **2018**, *71*, 3077–3087. [\[CrossRef\]](#)
129. Mazaheri, H.; Aval, H.J.; Jamaati, R. Enhancement of the Strength–Ductility Balance in Cu–40 Pct Zn Alloy by Single Roll Drive Rolling and Cooling-Assisted Friction Stir Processing. *Metall. Mater. Trans. A Phys. Metall. Mater. Sci.* **2023**, *54*, 2759–2770. [\[CrossRef\]](#)
130. Girish, G. Effect of rapid cooling on the properties of friction stir processed AA7075. *Proc. Inst. Mech. Eng. Part C J. Mech. Eng. Sci.* **2023**, *237*, 5975–5981. [\[CrossRef\]](#)
131. Huang, L.; Paidar, M.; Mohd Zain, A.; Refaai, M.R.A.; Abdullaev, S.; Šlapáková, M. Effect of processing environment during friction stir processing of AZ31/(ZrO₂ + CuO)p surface composite on the mechanical and tribological performance. *J. Mater. Res. Technol.* **2024**, *28*, 1891–1899. [\[CrossRef\]](#)
132. Sonar, T.; Lomte, S.; Gogte, C. Cryogenic Treatment of Metal—A Review. *Mater. Today Proc.* **2018**, *5*, 25219–25228. [\[CrossRef\]](#)
133. Trojovský, P.; Dhasarathan, V.; Boopathi, S. Experimental investigations on cryogenic friction-stir welding of similar ZE42 magnesium alloys. *Alexandria Eng. J.* **2023**, *66*, 1–14. [\[CrossRef\]](#)
134. Park, Z.S.; Kim, J.; Woo, Y.Y.; Lee, H.; Kim, J.H.; Moon, Y.H. Forced circulation of nitrogen gas for accelerated and eco-friendly cooling of metallic parts. *Appl. Sci.* **2019**, *9*, 3679. [\[CrossRef\]](#)
135. Ma, M.; Lai, R.; Qin, J.; Wang, B.; Liu, H.; Yi, D.; Zhai, T. Achieving exceptionally tensile properties and damage tolerance of 5083 aluminum alloy by friction stir processing assisted by ultrasonic and liquid nitrogen field. *Mater. Sci. Eng. A* **2021**, *806*, 140824. [\[CrossRef\]](#)
136. Rathinasuriyan, C.; Sankar, R. Wear and Corrosion Behavior of Cryogenic Friction Stir Processed AZ31B Alloy. *J. Mater. Eng. Perform.* **2021**, *30*, 3118–3128. [\[CrossRef\]](#)
137. Wang, Y.; Fu, R.; Zhou, X.; Thompson, G.B.; Yu, Z.; Li, Y. Enhanced mechanical properties of pure copper with a mixture microstructure of nanocrystalline and ultrafine grains. *Mater. Lett.* **2016**, *185*, 546–549. [\[CrossRef\]](#)
138. Singh Sidhu, H.; Singh, B.; Kumar, P. Effect of cryogenic treatment on corrosion behavior of friction stir processed magnesium alloy AZ91. *Mater. Today Proc.* **2021**, *46*, 10389–10395. [\[CrossRef\]](#)
139. Cao, F.; Sun, T.; Hu, J.; Hou, W.; Huang, G.; Shen, Y.; Ma, N.; Geng, P.; Hu, W.; Qu, X. Enhanced mechanical and anticorrosion properties in cryogenic friction stir processed duplex stainless steel. *Mater. Des.* **2023**, *225*, 111492. [\[CrossRef\]](#)
140. Wang, Y.; Fu, R.; Li, Y.; Zhao, L. A high strength and high electrical conductivity Cu–Cr–Zr alloy fabricated by cryogenic friction stir processing and subsequent annealing treatment. *Mater. Sci. Eng. A* **2019**, *755*, 166–169. [\[CrossRef\]](#)
141. Khodabakhshi, F.; Gerlich, A.P.; Simchi, A.; Kokabi, A.H. Cryogenic friction-stir processing of ultrafine-grained Al–Mg–TiO₂ nanocomposites. *Mater. Sci. Eng. A* **2015**, *620*, 471–482. [\[CrossRef\]](#)
142. Ammouri, A.H.; Kridli, G.T.; Ayoub, G.; Hamade, R.F. Investigating the effect of cryogenic pre-cooling on the friction stir processing of AZ31B. *Lect. Notes Eng. Comput. Sci.* **2014**, *2*, 1137–1140.
143. Thompson, B.; Doherty, K.; Su, J.; Mishra, R. Nano-sized grain refinement using friction stir processing. In *Friction Stir Welding and Processing VII*; John Wiley & Sons: Hoboken, NJ, USA, 2016; pp. 9–19. [\[CrossRef\]](#)
144. Ramaiyan, S.; Chandran, R.; Santhanam, S.K.V. Effect of Cooling Conditions on Mechanical and Microstructural Behaviours of Friction Stir Processed AZ31B Mg Alloy. *Mod. Mech. Eng.* **2017**, *7*, 144–160. [\[CrossRef\]](#)

145. Orozco-Caballero, A.; Álvarez-Leal, M.; Ruano, O.A.; Carreño, F. Improving the mechanical properties of a WE54 magnesium alloy through severe friction stir processing and rapid cooling. *Mater. Sci. Eng. A* **2022**, *856*, 143963. [[CrossRef](#)]
146. Godasu, A.K.; Kumar, A.; Mula, S. Influence of cryocooling on friction stir processing of Al-5083 alloy. *Mater. Manuf. Process.* **2020**, *35*, 202–213. [[CrossRef](#)]
147. Kumar, A.; Godasu, A.K.; Pal, K.; Mula, S. Effects of in-process cryocooling on metallurgical and mechanical properties of friction stir processed Al7075 alloy. *Mater. Charact.* **2018**, *144*, 440–447. [[CrossRef](#)]
148. Esmaily, M.; Shokuhfar, A. Ultra fine grain via friction stir processing of 7075-T6 grade aluminum alloy. *Defect Diffus. Forum* **2010**, *297–301*, 1116–1121. [[CrossRef](#)]
149. Kumar, A.; Pal, K.; Mula, S. Effects of cryo-FSP on metallurgical and mechanical properties of stir cast Al7075–SiC nanocomposites. *J. Alloys Compd.* **2021**, *852*, 156925. [[CrossRef](#)]
150. Khorrami, M.S.; Kazeminezhad, M.; Miyashita, Y.; Saito, N.; Kokabi, A.H. Influence of ambient and cryogenic temperature on friction stir processing of severely deformed aluminum with SiC nanoparticles. *J. Alloys Compd.* **2017**, *718*, 361–372. [[CrossRef](#)]
151. Tharwan, M.Y.; Hadidi, H.M. Experimental investigation on the thermal performance of a heat sink filled with PCM. *Alexandria Eng. J.* **2022**, *61*, 7045–7054. [[CrossRef](#)]
152. Patel, V.; Li, W.; Liu, X.; Wen, Q.; Su, Y.; Shen, J.; Fu, B. Tailoring grain refinement through thickness in magnesium alloy via stationary shoulder friction stir processing and copper backing plate. *Mater. Sci. Eng. A* **2020**, *784*, 139322. [[CrossRef](#)]
153. Mahmoud, E.R.I.; Khan, S.Z.; Aljabri, A.; Almohamadi, H.; Elkotb, M.A.; Gepreel, M.A.; Ebied, S. Free Intermetallic Cladding Interface between Aluminum and Steel through Friction Stir Processing. *Crystals* **2022**, *12*, 1413. [[CrossRef](#)]
154. Patel, M.; Murugesan, J. Effect of the Tool Pin Eccentricity and Cooling Rate on Microstructure, Mechanical Properties, Fretting Wear, and Corrosion Behavior of Friction Stir Processed AA6063 Alloy. *J. Mater. Eng. Perform.* **2022**, *31*, 8554–8566. [[CrossRef](#)]
155. MD, F.K.; Karthik, G.M.; Panigrahi, S.K.; Janaki Ram, G.D. Friction stir processing of QE22 magnesium alloy to achieve ultrafine-grained microstructure with enhanced room temperature ductility and texture weakening. *Mater. Charact.* **2019**, *147*, 365–378. [[CrossRef](#)]
156. MD, F.K.; Panigrahi, S.K. Achieving excellent superplasticity in an ultrafine-grained QE22 alloy at both high strain rate and low-temperature regimes. *J. Alloys Compd.* **2018**, *747*, 71–82. [[CrossRef](#)]

Disclaimer/Publisher’s Note: The statements, opinions and data contained in all publications are solely those of the individual author(s) and contributor(s) and not of MDPI and/or the editor(s). MDPI and/or the editor(s) disclaim responsibility for any injury to people or property resulting from any ideas, methods, instructions or products referred to in the content.